# Export-deficient monoubiquitinated PEX5 triggers peroxisome removal in SV40 large T antigen-transformed mouse embryonic fibroblasts

**Marcus Nordgren,[1] Tânia Francisco,[2] Celien Lismont,[1] Lore Hennebel,[1] Chantal Brees,[1] Bo Wang,[1] Paul P. Van Veldhoven,[1] Jorge E. Azevedo,[2,3] Marc Fransen[1,*]**

[1] Laboratory of Lipid Biochemistry and Protein Interactions, Department of Cellular and Molecular Medicine, University of Leuven – KU Leuven, Leuven, Belgium; [2] Instituto de Biologia Molecular e Celular, Universidade do Porto, Porto, Portugal; and [3] Instituto de Ciências Biomédicas Abel Salazar, Universidade do Porto, Porto, Portugal

[*]***Corresponding author:*** Dr. Marc Fransen, Laboratory of Lipid Biochemistry and Protein Interactions, Department of Cellular and Molecular Medicine, University of Leuven – KU Leuven, Herestraat 49 box 601, 3000 Leuven, Belgium. Tel.: +32 16 330114; Fax: +32 16 330642; E-mail address: marc.fransen@med.kuleuven.be

**Keywords:** peroxisome, PEX5, pexophagy, protein import, receptor recycling, selective autophagy, ubiquitin

**Running Title:** PEX5-mediated peroxisome removal

**Abbreviations:** 3-MA, 3-methyladenine; ABCD3/PMP70, ATP-binding cassette, sub-family D (ALD), member 3; ATG, autophagy-related; DTM, docking/translocation machinery; EGFP, enhanced green fluorescent protein; Hs, *homo sapiens*; KR, KillerRed; LAMP, lysosomal-associated membrane protein; MAP1LC3A/B, microtubule-associated protein 1 light chain 3 alpha/beta; MEFs, mouse embryonic fibroblasts; Mm, *Mus musculus*; NBR1,

neighbor of BRCA1 gene 1; OPTN, optineurin; PEX, peroxisomal biogenesis factor; PMP, peroxisomal membrane protein; PNS, postnuclear supernatant; PtdIns3K, class III phosphatidylinositol 3-kinase; PTS, peroxisomal targeting signal; REM, receptor export machinery; ROS, reactive oxygen species; SLC25A17, solute carrier family 25 (mitochondrial carrier; peroxisomal membrane protein, 34kDa), member 17; SQSTM1, sequestosome 1; SV40T, SV40 large T antigen-transformed; TPR, tetratricopeptide repeat; Ub, ubiquitin

## Abstract

Peroxisomes are ubiquitous cell organelles essential for human health. To maintain a healthy cellular environment, dysfunctional and superfluous peroxisomes need to be selectively removed. Although emerging evidence suggests that peroxisomes are mainly degraded by pexophagy, little is known about the triggers and molecular mechanisms underlying this process in mammalian cells. In this study, we show that PEX5 proteins fused to a bulky C-terminal tag trigger peroxisome degradation in SV40 large T antigen-transformed mouse embryonic fibroblasts. In addition, we provide evidence that this process is autophagy-dependent and requires monoubiquitination of the N-terminal cysteine residue that marks PEX5 for recycling. As our findings also demonstrate that the addition of a bulky tag to the C terminus of PEX5 does not interfere with PEX5 monoubiquitination but strongly inhibits its export from the peroxisomal membrane, we hypothesize that such a tag mimics a cargo protein that cannot be released from PEX5, thus keeping monoubiquitinated PEX5 at the membrane for a sufficiently long time to be recognized by the autophagic machinery. This in turn suggests that monoubiquitination of the N-terminal cysteine of peroxisome-associated PEX5 not only functions to recycle the peroxin back to the cytosol, but also serves as a quality control mechanism to eliminate peroxisomes with a defective protein import machinery.

# Introduction

To maintain a healthy intracellular environment, cells need to eliminate excessive and dysfunctional organelles. This turnover mainly occurs within the lysosome in a process called autophagy. Currently, 3 major autophagy pathways have been characterized in eukaryotic cells: macroautophagy, microautophagy, and chaperone-mediated autophagy.[1-3] During macroautophagy—hereafter simply referred to as autophagy—a cup-shaped double membrane-bound structure, called the phagophore, is formed in the cytoplasm. This structure elongates to engulf the cargo and eventually becomes a cargo-laden short-lived organelle known as the autophagosome. The intra-autophagosomal components are, upon autophagosome-lysosome fusion, finally degraded by lysosomal hydrolases.

Autophagy is mainly mediated by AuTophaGy-related (ATG) proteins, of which at least 38 have been identified in yeast.[4,5] Of these, less than half are thought to be required for canonical autophagy, which is a highly conserved process among eukaryotes.[4] Autophagy occurs both selectively and nonselectively, and—in contrast to bulk autophagy—selective autophagy pathways require the additional specific action of autophagy receptors (e.g., SQSTM1/p62, NBR1, and OPTN).[6,7] These receptors act independently, or concertedly, to bridge substrates targeted for degradation with the elongating phagophore via tethering of both structures. Substrate binding generally occurs through a ubiquitin-binding domain, and the binding to the phagophore via an LC3-interacting region.[7] Microtubule-associated protein 1 light chain 3 alpha (MAP1LC3A) and its homologs are present on the phagophore convex and concave membranes, where they—among other functions—mediate the specificity of selective autophagy.[7]

Peroxisomes are dynamic organelles that rapidly adapt their size, protein content, and number in response to altering environmental conditions. Important functions of peroxisomes in mammals include α- and β-oxidation of fatty acids and the biosynthesis of plasmalogens

and docosahexaenoic acid.[8-10] Importantly, as (i) peroxisomal enzymes produce vast amounts of reactive oxygen species (ROS) as part of their catalytic cycle,[11] and (ii) ROS are involved in an array of signaling pathways,[12] these organelles are also increasingly being recognized as important redox signaling platforms.[13,14]

To perform their various functions, peroxisomes require an operational and efficient import machinery for matrix proteins. The vast majority of these proteins contain a peroxisomal targeting signal type 1 (PTS1), made up of a C-terminally located tripeptide with the consensus sequence (S/A/C)-(K/R/H)-(L/A) (in single-letter amino acid code).[15,16] PTS1-containing proteins are recognized in the cytosol by the peroxisomal matrix protein import receptor PEX5, which interacts with the PTS1 via 6 tetratricopeptide repeats (TPRs) that are located in its C terminus.[17] Importantly, the mammalian *PEX5* transcript undergoes alternative splicing yielding 2 major isoforms, PEX5(S) (the short variant) and PEX5(L) (the long variant), the latter of which is also involved in PTS2-import.[18] Upon cargo recognition, the protein complex is transported to the peroxisomal membrane where PEX5 docks on the docking/translocation machinery (DTM), consisting of the peroxins PEX13, PEX14, and the 3 RING proteins PEX2, PEX10, and PEX12.[19,20] The PEX5-cargo protein complex is then inserted into the DTM with the concomitant translocation of the cargo protein into the organelle matrix. Finally, DTM-inserted PEX5 is monoubiquitinated on an evolutionarily conserved cysteine residue (in humans and mice at amino acid position 11) and subsequently extracted from the peroxisomal membrane in an ATP-dependent manner by the receptor export machinery.[21,22] This machinery, often called 'REM'[23] or 'exportomer',[24] consists in mammals of the core proteins PEX1 and PEX6, 2 $AAA^+$ ATPases that can interact and form a heterohexameric ring complex.[25,26]

Over the last decades, it has become increasingly clear that mammalian peroxisomes are degraded via selective autophagy (a process known as 'pexophagy').[27-32] This is perhaps

best illustrated by the observation that proliferated rat peroxisomes are rapidly turned over in an autophagy-dependent manner upon removal of the proliferation stimulus.[27,28] Unfortunately, little is currently known about the physiological triggers and molecular mechanisms underlying mammalian pexophagy. However, since (i) peroxisomes—like mitochondria—produce large amounts of ROS as part of their metabolism,[11] (ii) excessive organelle-specific ROS-generation causes mitochondria- and endoplasmic reticulum-selective degradation in mammalian cells,[33-35] and (iii) highly oxidized peroxisomes can be degraded via pexophagy in *Hansenula polymorpha* and *Arabidopsis thaliana*,[36,37] it is tempting to speculate that mammalian pexophagy can be triggered via ROS-related mechanisms.

Finally, accumulating evidence points towards an integral role of ubiquitin in the targeting of mammalian peroxisomes to autophagosomes.[30,32,38] For example, ectopic expression of peroxisomal membrane proteins (PMPs) attached to cytosolically exposed ubiquitin triggers pexophagy in a SQSTM1-dependent manner.[38] In addition, overexpression of both NBR1 and PEX3 has been demonstrated to induce pexophagy in a ubiquitin-dependent fashion.[30,32] However, endogenous PMPs that are ubiquitinated during pexophagy have not yet been identified. Nevertheless, a proposed candidate is PEX5,[30,39] which—as mentioned above—is known to be monoubiquitinated on a cysteine residue (Cys11 in human and mouse PEX5) at the peroxisomal membrane during its normal import cycle.[21] In addition, it has recently been shown that cytosolic PEX5 can also be ubiquitinated at Lys527, probably the result of a yet uncharacterized quality control process.[40] In this study, we provide evidence that expression of Cys11-monoubiquitinatable but export-deficient variants of PEX5 trigger peroxisome degradation in SV40 large T antigen-transformed (SV40T) mouse embryonic fibroblasts (MEFs). This finding strongly indicates that the amount of Cys11-monoubiquitinated PEX5 at the peroxisomal membrane may function as a quality control mechanism to eliminate peroxisomes with a defective/jammed protein import machinery.

## Results

### Expression of PEX5 proteins fused to a bulky C-terminal tag triggers peroxisome removal in SV40T-MEFs

To gain more insight into potential triggers for peroxisome degradation in mammalian cells, we first tested the hypothesis that these organelles can be selectively removed upon oxidative damage. To generate oxidative stress in the peroxisomal matrix or at the peroxisomal membrane in a temporally controlled manner, we designed a set of KillerRed (KR)-fusion proteins. KR is a genetically-encoded photosensitizer that generates ROS upon green light illumination.[41] Intriguingly, although we were unable to show an increase in peroxisome turnover upon photoactivation of peroxisomal matrix-targeted KR,[42] we found that overexpression of nonphotoactivated human (*Homo sapiens*, Hs) PEX5(L)-KR in SV40T-MEFs already resulted in a partial or complete disappearance of peroxisomes in a large number of cells, as detected by immunofluorescence with anti-PEX14 antibodies (**Fig. 1A**). As such a phenotype was not discernible in cells overexpressing only PEX5(L) or KR (**Fig. 1B and C**, respectively), we next investigated whether or not overexpression of other PEX5-fusion proteins could also induce peroxisome removal. Note that, to facilitate the identification of transfected cells, the indicated test plasmids were routinely cotransfected with a plasmid encoding mitochondria-targeted EGFP. In addition, to quantify and compare the results in an easy and reliable way, the number of peroxisomes in each transfected cell was counted and catalogued as more than 50 (no or moderate reduction in peroxisome number), between 1 and 50 (strong reduction in peroxisome number), or none (complete absence of peroxisomes).

A first set of experiments, in which peroxisome number was analyzed with ABCD3/PMP70-antibodies (**Fig. 2A**), revealed that (i) also PEX5(S)-EGFP—but not EGFP-PEX5(S) or PEX5(S)-FLAG—could trigger peroxisome removal, (ii) the PEX5-EGFP-

mediated removal process of peroxisomes was PEX5 splice-variant independent, and (iii) this process could be triggered by both human and mouse PEX5(L) (**Fig. 2B**). Co-expression of mt-EGFP had no effect on the outcome of the experiment (**Fig. S1**). To eliminate the possibilities that overexpression of PEX5-EGFP resulted in the masking of the PEX14 and ABCD3 epitopes or the selective degradation of these PMPs, we also carried out immunostainings with antibodies recognizing either CAT/catalase or a mix of peroxisomal matrix proteins (ab-MF16). The results of these experiments clearly showed that also peroxisomal matrix proteins disappeared upon PEX5(L)-EGFP expression (**Fig. S2**), thereby confirming and extending our initial observations.

In a subsequent series of experiments, we obtained evidence that the degree of peroxisome removal could be correlated with the expression levels of PEX5-EGFP (**Fig. S3**) and that this process steadily increased up to 20 h post-transfection, after which no further increase was observed (**Fig. S4**). Finally, as KR is a dimeric protein and EGFP has a weak tendency to dimerize,[43] we also checked the peroxisome removal capacity of PEX5-mCherry and PEX5-HaloTag (mCherry and HaloTag tags are strictly monomeric tags) and observed that also these PEX5-fusion proteins could induce peroxisome removal (**Fig. S5**). Taken together, these data clearly show that the presence of a bulky tag at the C terminus of PEX5 can trigger peroxisome degradation in SV40T-MEFs in a time- and expression level-dependent manner.

**PEX5-EGFP-induced peroxisome removal is dependent on autophagy**

As autophagy is thought to be the responsible mechanism for most, if not all, peroxisome turnover in mammalian cells,[29,31] we next investigated the potential involvement of this pathway in PEX5-EGFP-mediated peroxisome degradation. For this purpose, we employed SV40 large T antigen-transformed *atg5*$^{-/-}$ MEFs as well as control MEFs treated with the autophagy inhibitors 3-methyladenine (3-MA) or LY294002: ATG5 is essential for

efficient MAP1LC3-lipidation, a crucial step in the formation of canonical autophagosomes;[44] and 3-MA and LY294002 are inhibitors of class I phosphoinositide 3-kinases and class III phosphatidylinositol 3-kinases (PtdIns3Ks) that suppress autophagosome formation via inhibition of the class III enzyme.[45] Importantly, as both PtdIns3K inhibitors (**Fig. 3A**) as well as ATG5 inactivation (**Fig. 3B**) interfered with PEX5-EGFP-induced peroxisome removal, the observed phenotype is highly likely to be autophagy dependent. In this context, it is also interesting to mention that—despite the fact that peroxisome removal was not completely blocked in *atg5*$^{-/-}$ cells—PEX5-EGFP behaved similarly to SLC25A17-Ub, a non-natural protein already reported to selectively trigger peroxisome removal in mammalian cells in an autophagy-dependent manner (**Fig. 3C**).[38] Taken together, these data strongly point towards autophagy as the major mechanism for PEX5-EGFP-induced peroxisome removal.

Nevertheless, and despite repeated efforts, we were unable to colocalize peroxisomes with endogenous LC3 or LAMP1 (lysosomal-associated membrane protein 1) nor with recombinant EGFP-LC3, LAMP1-EGFP, or LAMP2A-EGFP, not even in the presence of chloroquine (a lysosomal lumen alkalizer) or protease inhibitor mixtures of N-(trans-epoxysuccinyl)-L-leucine 4 guanidinobutylamide (E-64), pepstatin A and/or leupeptin (data not shown). Potential explanations for these negative results may be that the percentage of (GFP-)LC3 involved in PEX5-EGFP-induced peroxisome removal and the amount of peroxisomal markers trapped within the lysosomal compartment are simply below the detection limit. Regarding the latter, it is important to note that, as (i) the peroxisomal volume in mammalian cells is ≤1% of the total cellular volume,[46] and (ii) the PEX5-EGFP-induced removal of the peroxisome population was spread over 20 h (**Fig. S4**), the presence of even a minor residual protease activity may be sufficient to prevent the detection of peroxisomal marker proteins in lysosomes. In addition, as even low concentrations of chloroquine (e.g., 20

μM) cause a dramatic expansion of the lysosomal compartment, signal dilution effects need also to be taken into account.

To rule out the possibility that the observed decrease in peroxisome number was not a direct result of high basal turnover rates in combination with a reduction in peroxisome formation, we also performed a series of pulse-chase labeling experiments to estimate the basal turnover rate of peroxisomes in SV40T-MEFs (peroxisomes are continually formed and degraded, and the actual number of these organelles within a cell depends on the kinetics of both processes). However, as could be expected from similar studies performed in Chinese hamster ovary cells,[47] the basal turnover rate of peroxisomes was not high enough to consider a reduction in peroxisome formation as the causal factor for the PEX5-EGFP-induced phenotype (**Fig. S6**). In this context, it is also worth noting that, under basal conditions, the number of peroxisomes was not statistically different ($p<0.01$) between any of the SV40T-MEFs under study (**Fig. S7**).

Finally, we also investigated whether or not PEX5-EGFP expression activated general autophagy. As these studies revealed that such expression did not lead to an increase in the average number of MAP1LC3B puncta per cell (data not shown) or to differences in the amount of LC3-II between samples in the presence or absence of the vacuolar-type ATPase inhibitor bafilomycin $A_1$ (**Fig. S8**; for reasons that will become clear later, $PEX5_{C11A}$-EGFP was included as a negative control), PEX5-EGFP expression did not seem to affect the overall autophagic flux. This idea was further corroborated by the observation that expression of this protein selectively eliminated peroxisomes and had no effect on the normal distribution and morphology of the endoplasmic reticulum and mitochondria (**Fig. S9**).

**The N-terminal cysteine residue that marks PEX5 for recycling is crucial for PEX5-EGFP-induced pexophagy**

As (i) it has been hypothesized that ubiquitination of endogenous proteins at the peroxisomal membrane may trigger peroxisome removal in mammalian cells,[30,32,38] and (ii) PEX5 export requires monoubiquitination of the protein at Cys11,[21] we next examined whether or not 2 N-terminally truncated (PEX5(S)$_{\Delta N16}$ and PEX5(S)$_{\Delta N110}$) variants of PEX5 lacking this cysteine residue could still induce peroxisome degradation. Since these experiments clearly showed that a deletion of the first 16 amino acid residues in PEX5 is sufficient to disrupt PEX5-EGFP-induced peroxisome removal (**Fig. 4A**), we performed another series of experiments in which we tested the capability of PEX5(L)$_{C11K}$-EGFP, PEX5(L)$_{C11S}$, PEX5(L)$_{C11S}$-EGFP, PEX5(L)$_{C11A}$, and PEX5(L)$_{C11A}$-EGFP to trigger peroxisome removal. Note that (i) PEX5(L)$_{C11K}$ is a monoubiquitinatable and fully functional variant of PEX5 in which Cys11 has been substituted by a lysine,[48] (ii) PEX5(L)$_{C11S}$ is an export-incompetent PEX5 mutant in which Cys11 has been replaced by a serine, an amino acid residue that can be slowly ubiquitinated under specific conditions,[49,50] and (iii) PEX5(L)$_{C11A}$ is also an export-incompetent PEX5 mutant in which Cys11 has been exchanged for an alanine, a nonubiquitinatable amino acid.[48,51] As shown in **Fig. 4B**, expression of PEX5(L)$_{C11K}$-EGFP, PEX5(L)$_{C11S}$-EGFP, and PEX5(L)$_{C11A}$-EGFP respectively caused a strong, moderate, or no pexophagy phenotype in most transfected cells, strongly indicating that the presence of a ubiquitinatable residue at amino acid position 11 of PEX5 is crucial for PEX5-EGFP-induced peroxisome removal. Note that further analysis of the key variants of PEX5-EGFP demonstrated that these proteins were all partially localized to peroxisomes (**Fig. S10**) and expressed to a similar extent (**Fig. S11**). Interestingly, expression of nontagged PEX5(L)$_{C11S}$, but not PEX5(L)$_{C11A}$, also triggered peroxisome degradation in a small number of cells (**Fig. 4B**). Although the reason for this phenomenon is not yet clear (but see Discussion), this result further supports the importance of a ubiquitinatable residue at amino acid position 11 of PEX5 to trigger peroxisome removal.

Finally, we also tested the ability of PEX5(L)$_{N526K}$-EGFP, PEX5(L)$_{K527R}$-EGFP, and PEX5(S)$_{\Delta C299}$-PEX5(L)/PEX5R$_{\Delta N326}$-EGFP to induce peroxisome removal in our experimental setup. PEX5(L)$_{N526K}$ and PEX5(L)$_{K527R}$ are PEX5 mutants that are incapable of binding PTS1 proteins or undergo lysine-linked monoubiquitination, respectively,[17,40] and PEX5(S)$_{\Delta C299}$-PEX5L/PEX5R$_{\Delta N324}$-EGFP is a chimeric protein composed of the N-terminal 298 amino acids of PEX5(S) and the C-terminal TPR-containing domain (amino acids 325 to 624) of PEX5L/PEX5R (peroxisomal biogenesis factor 5-like), a PEX5-related PTS1-binding protein.[52] As the PEX5(L)$_{N526K}$ and PEX5(L)$_{K527R}$ mutants did not lose their capacity to trigger PEX5-mediated peroxisome degradation (**Fig. 4C**), it can be concluded that neither PTS1 binding nor monoubiquitination of PEX5(L) at Lys527 were essential for this process. In addition, from the results obtained with the chimeric PEX5(S)$_{\Delta C299}$-PEX5L/PEX5R$_{\Delta N326}$-EGFP protein (**Fig. 4C**), it was clear that—although the primary amino acid sequence of the TPRs clearly influenced the peroxisome removal phenotype—the TPRs of PEX5 were not essential for PEX5-EGFP-triggered peroxisome removal. In summary, these data provide direct evidence that the N-terminal cysteine residue that marks PEX5 for recycling is crucial for PEX5-mediated peroxisome removal.

**C-terminal tagging with EGFP renders PEX5 export-incompetent and leads to the accumulation of Ub-PEX5-EGFP at the peroxisomal membrane**

As previous work has pointed out that (i) the accumulation of monoubiquitinated membrane proteins on the cytosolic surface of peroxisomes can cause pexophagy,[38,39] and (ii) Cys11-ubiquitination of PEX5 regulates its ATP-dependent export from peroxisomes back to the cytosol,[21,51] we here investigated the dynamics and topology of PEX5(L)-EGFP at the peroxisomal membrane by employing a previously described *in vitro* import/export assay.[21] In short, we incubated radiolabeled PEX5(L), PEX5(L)-EGFP, PEX5(L)$_{C11S}$-EGFP, and PEX5(L)$_{C11A}$-EGFP with a (peroxisome-containing) rat liver postnuclear supernatant fraction

supplemented with ATP or AMP-PNP and either Ub or GST-Ub. Organelle and/or supernatant fractions were then treated or not with proteinase K, processed for SDS-PAGE under nonreducing or reducing conditions, and assayed by autoradiography. Recall that (i) during its transient passage through the peroxisomal membrane, PEX5 adopts a transmembrane topology, only exposing a protease-accessible N-terminal domain of approximately 2 kDa to the cytosol, (ii) monoubiquitination of PEX5 exclusively occurs when the receptor is embedded in the DTM, (iii) substitution of Cys11 by Ser or Ala results in PEX5 proteins that are still functional in docking and membrane insertion but are largely or completely incompetent in the ubiquitination/export process, respectively, and (iv) AMP-PNP, a nonhydrolyzable analog of ATP, blocks the export of monoubiquitinated PEX5 back into the cytosol.[48,53]

In a first series of experiments, we found that PEX5(L)-EGFP entered the DTM and became monoubiquitinated similar to nontagged PEX5(L) (**Fig. 5A**, left panels, compare the AMP-PNP conditions). However, we also observed that Ub-PEX5(L)-EGFP, in contrast to Ub-PEX5(L), encountered difficulties in leaving the DTM (same panels, compare the ATP conditions), a property that can be better appreciated using a 2-step import/export assay (**Fig. 5B**). In these assays, radiolabeled PEX5(L) and PEX5(L)-EGFP were first imported in the presence of AMP-PNP. The organelles were then sedimented and the supernatant fraction (containing nonimported PEX5 proteins) was discarded. Finally, the organelles were resuspended in fresh ATP-containing import buffer and incubated for 5 min at 37°C to promote export of the monoubiquitinated species. As shown in **Fig. 5B**, the vast majority of monoubiquitinated PEX5(L)-EGFP remained in the organelle fraction, in contrast to PEX5(L), which was recovered mainly in the soluble fraction. PEX5(L)$_{C11S}$-EGFP and PEX5(L)$_{C11A}$-EGFP could also efficiently enter the DTM (**Fig. 5A**, right panels). Nonetheless, as these molecules are respectively poor substrates or not substrates for monoubiquitination,

297 they became trapped at the DTM, even in the presence of ATP. Note that, as (i) PEX5(L)$_{C11S}$-
298 EGFP and PEX5(L)$_{C11A}$-EGFP were not posttranslationally modified at the peroxisomal
299 membrane (**Fig. 5A**, right panels), (ii) replacement of Ub with GST-Ub resulted in higher
300 molecular weight species of PEX5(L) and PEX5(L)-EGFP (**Fig. 5C**, upper panels), and (iii)
301 treatment of the protein samples with DTT destroyed the thioester bond between (GST-)Ub
302 and PEX5(L)(-EGFP) (**Fig. 5C**, lower panels; see also **Fig. S12**), it is clear that the PEX5(L)
303 modifications in our assays represent Cys11-dependent monoubiquitination events.

304 In a second series of experiments, we found that organelle-bound (Ub-)PEX5(L) and
305 (Ub-)PEX5(L)-EGFP displayed a similar topology, as assessed by protease-protection assays.
306 Indeed, in the presence of ATP or AMP-PNP, we respectively detected (i) small amounts of
307 PEX5(L) and PEX5(L)-EGFP exposing the majority of their mass in the peroxisomal matrix
308 (**Fig. 6**, upper panel, lanes 2 and 5, arrowheads labeled 'a'), and (ii) large amounts of DTM-
309 embedded Ub-PEX5(L) and Ub-PEX5(L)-EGFP (**Fig 6**, upper panel, lanes 3 and 6,
310 arrowheads labeled 'b'). At first sight, this finding may be counterintuitive given our earlier
311 observation that, in the presence of ATP, Ub-PEX5(L)-EGFP was more abundant in the
312 organellar fraction than Ub-PEX5(L) (**Fig. 5A**, compare lane 2 in the 2 upper panels).
313 However, a careful analysis of the autoradiographs that are shown in **Fig. 6** revealed that a
314 major fraction of Ub-PEX5(L)-EGFP obtained in the presence of ATP was accessible to
315 proteinase K, whereas the one obtained in the presence of AMP-PNP was not. Indeed, in the
316 condition with ATP, we observed 3 additional protease-resistant PEX5(L)-EGFP fragments
317 around 35 kDa (**Fig. 6**, see asterisks). Note that these fragments contained the EGFP moiety
318 of the chimeric protein because they were recognized by an anti-EGFP antibody (see **Fig.**
319 **S13**). In addition, as they could not be observed for export-incompetent PEX5(L)$_{C11A}$-EGFP
320 (**Fig. 6**, upper and lower panels, 2 last lanes), our findings strongly indicate that the REM is

capable of extracting PEX5-EGFP partially out of the DTM, but most likely becomes jammed when it encounters a tightly folded domain (e.g., EGFP or KR).

**PEX5-EGFP is monoubiquitinated *in cellulo* in a Cys11-dependent manner**

To find evidence that PEX5-EGFP is also monoubiquitinated at Cys11 when expressed in SV40T-MEFs, whole lysates of cells expressing $PEX5_{C11A}$-EGFP or PEX5-EGFP were subjected to SDS-PAGE under nonreducing and reducing conditions and processed for immunoblotting with antibodies against PEX5. From these experiments, it is clear that a small portion of PEX5-EGFP was posttranslationally modified upon expression in these cells (**Fig. S14**). In addition, as (i) this modification is Cys11-dependent, DTT-sensitive, and caused a molecular shift of approximately 8 kDa (**Fig. S14**), (ii) this behavior mimics that of PEX5-EGFP *in vitro* (**Figs. 5 and S12**), and (iii) previous studies have shown that, in mammals, the DTT-sensitive form (with monoubiquitination at the conserved cysteine residue) is associated with peroxisomes and the DTT-insensitive form (with unknown modification) is located in the cytosol,[40,48;51,54] it is reasonable to conclude that the posttranslationally-modified form of PEX5-EGFP represents peroxisome-associated ubiquitinated PEX5-EGFP.

Next, as expression of PEX5-EGFP is expected to lead to an accumulation of Ub-PEX5-EGFP at the peroxisomal membrane, we also checked whether or not PEX5-EGFP-expressing cells contain ubiquitin-positive peroxisomes. Unfortunately, despite the fact that we used 2 different anti-ubiquitin antibodies, including one that was already successfully used by others to visualize ubiquitin-positive peroxisome clusters in PEX3-HA2-overexpressing cells,[32] no ubiquitin-positive peroxisomes could be detected, not even upon treatment of the cells with 3-MA (data not shown). However, (i) the ubiquitin-moieties in DTM-embedded PEX5-EGFP molecules may be shielded by potential interaction partners (e.g., PEX1, or PEX6), (ii) in contrast to what happens in PEX3-HA2 overexpressing cells, the fluorescence

intensity of putative ubiquitin-positive peroxisomes is not enhanced because the organelles do not cluster upon expression of PEX5-EGFP, and (iii) ubiquitin is also ligated to a great number of endogenous proteins, the threshold for detection of ubiquitin-positive peroxisomes may be below the limit needed to visualize such structures above background fluorescence.

**The PEX5-EGFP-induced phenotype is cell type-specific**

We also expressed PEX5-EGFP in other mammalian cell types (e.g., human skin fibroblasts, rat embryonic fibroblasts, and a mouse oligodendrocyte cell line) and unexpectedly found that this protein could not trigger peroxisome removal in these cells (data not shown). In addition, we obtained empirical evidence that the PEX5-EGFP-induced peroxisome removal phenotype in MEFs can be directly linked to the SV40 large T antigen-induced immortalization of these cells. Indeed, expression of PEX5-EGFP quickly resulted in the disappearance of peroxisomes in SV40T-cells (e.g., "homemade" control MEFs,[55] *Atg5*$^{+/+}$ MEFs,[56] and *Perk*$^{+/+}$ MEFs,[57]), but not in primary control MEFs (passage <5)[55] and spontaneously transformed *Sqstm1*$^{+/+}$ MEFs.[58] Note that, as the expression levels of pEGFP-N1-encoded proteins are comparable in spontaneously transformed- and SV40T-cells, at least within the time scale of the experiments (**Fig. S15**), these differences in phenotype are caused by other factors than differences in PEX5-EGFP expression levels (see Discussion).

We still considered the possibility that PEX5-EGFP displays an export defect *in vivo* only in SV40T-cells and that the protein is actually functional in other cells. To test this possibility, PEX5-deficient human fibroblasts and spontaneously-transformed MEFs were subjected to transfection experiments to assess whether or not PEX5-EGFP has complementing or dominant-negative activity in peroxisomal matrix protein import. Appropriate controls (non-tagged $PEX5_{WT}$, $PEX5_{C11K}$, $PEX5_{C11S}$, and $PEX5_{C11A}$) were included to discriminate between different outcomes ($PEX5_{WT}$ and $PEX5_{C11K}$, but not $PEX5_{C11S}$ and $PEX5_{C11A}$, restore PTS1 protein import in PEX5-deficient cells; and $PEX5_{C11S}$

and $PEX5_{C11A}$, but not $PEX5_{WT}$ and $PEX5_{C11K}$, exert a dominant-negative activity on the same process in control cells).[48,51] From these experiments, it is clear that PEX5(L)-EGFP cannot restore peroxisomal matrix protein import in PEX5-deficient human fibroblasts (**Fig. S16A**) and interfered with PTS1 protein import upon expression in spontaneously transformed control MEFs (**Fig. S16B**).

**Downregulation of PEX1, SQSTM1, or NBR1 expression does not interfere with PEX5-EGFP-induced peroxisome removal**

To investigate the potential role of the PEX5 export machinery in PEX5-EGFP-induced peroxisome removal, we used Dicer substrate RNAs (DsiRNAs) to downregulate the expression level of PEX1, an essential REM component.[16] Note that, under the employed conditions (for details, see Materials and Methods), virtually all cells were transfected (as confirmed by a fluorescently-labeled scrambled control RNA duplex) (**Fig. S17**). Despite the fact that we could knock down PEX1 (**Fig. S18, panels A and B**), no effect could be observed on the level of the PEX5-EGFP-induced phenotype **(Fig. 7A**). In addition, such treatment did not affect peroxisome number in cells overexpressing HsPEX5 (**Fig. 7B**). Unfortunately, as additional experiments revealed that the residual amounts of PEX1 were sufficient to retain a functional PTS1 import machinery (**Fig. S18C**), no reliable conclusions can be drawn regarding the potential role of PEX1 in the process under study.

To investigate the potential role of the ubiquitin-binding selective autophagy receptors SQSTM1 and NBR1, a similar approach was used. Also here we could observe a significant downregulation of the expression levels of SQSTM1 (**Fig. S19, panels A and C**) and, albeit to a lesser extent, NBR1 (**Fig. S19, panels B and D**). Unfortunately, once again, we could not observe any effect on the level of PEX5-EGFP-induced peroxisome removal **(Fig. 7C**). The interpretation of these data is presented below.

## Discussion

In recent years, the phenomenon of selective organelle degradation has attracted increasing attention.[59-61] The main reason for this is that an accumulation of dysfunctional organelles contributes to developmental abnormalities, aging, inflammation, cancer and other diseases.[6] The pexophagy field has also gained much interest. However, despite rapid and considerable progress in our understanding of how peroxisomes are selectively degraded in (*Saccharomyces cerevisiae* and methylotrophic) yeasts,[29,62-65] little is known about how this process is regulated in mammalian cells.[31] This is perhaps best illustrated by the fact that, although it has been demonstrated that ectopic expression of PMPs attached to cytosolically exposed ubiquitin can trigger pexophagy,[38] endogenous PMPs that are ubiquitinated during pexophagy have not yet been identified. In this study, we show that expression of a monoubiquitinatable but export-incompetent variant of PEX5, a naturally monoubiquitinated protein, results in the accumulation of Ub-PEX5 at the peroxisomal membrane and triggers peroxisome removal in SV40T-MEFs. These observations provide the first strong evidence in favor of the recent hypothesis that alterations in PEX5 and ubiquitin dynamics on peroxisome membranes can regulate mammalian pexophagy.[30,39] The potential underlying molecular mechanisms of these findings and their implications for future research are discussed in the following paragraphs.

In our initial experiments aimed at clarifying whether or not peroxisomes can be selectively removed upon oxidative damage, we accidentally found that expression of PEX5 proteins fused to a bulky C-terminal tag (e.g., KR, EGFP, HaloTag, or mCherry) caused the disappearance of peroxisomes in SV40T-MEFs (**Figs. 1A, 2B, and S5**). In addition, we observed that this process required the presence of the N-terminal cysteine residue that marks PEX5 for recycling (**Fig. 4B**). As these observations, combined with the finding that PEX5 Cys11 monoubiquitination only takes place at the peroxisomal membrane,[21] strongly

indicated that the addition of a bulky tag to the C terminus of PEX5 interferes with the export step of the cycling receptor from the peroxisome to the cytosol, we employed a previously established *in vitro* assay[21] to study the import/export kinetics of PEX5-EGFP at the peroxisomal membrane. These experiments clearly demonstrated that PEX5-EGFP can enter the DTM and become monoubiquitinated at Cys11 as is the nontagged wild-type PEX5 (**Fig. 5**). However, in contrast to Ub-PEX5, Ub-PEX5-EGFP remained largely associated with the organelle pellet in the presence of ATP (**Fig. 5A, B**), clearly showing that the existence of a tightly folded domain at the C terminus of PEX5 interfered with its export back into the cytosol (**Fig. 5A, B**). Importantly, Ub-PEX5-EGFP was still a substrate for the REM. Indeed, this protein became partially accessible to proteinase K under conditions where the REM was active (i.e., when ATP but not AMP-PNP was used in the *in vitro* assays) yielding a set of organelle-associated protease-resistant fragments of approximately 35 kDa that comprise the bulky EGFP moiety (**Figs. 6 and S13**). The behavior of Ub-PEX5-EGFP can be explained in 2 ways. On the one hand, it is possible that PEX5 exits the DTM via a REM-dependent threading mechanism, and that—by analogy to some other $AAA^+$ ATPases[66]—tightly folded proteins such as EGFP (or a cargo protein that cannot be released from PEX5) cannot pass through a hole that may be present in the PEX1-PEX6 complex. Alternatively, it is conceivable that the DTM acts as a trap for globular proteins, letting them in but preventing them from getting out. Regardless of the mechanism, and although there is currently compelling evidence suggesting that the cargo release step occurs prior to monoubiquitination of PEX5,[19,67,68] the results presented here provide experimental evidence to support the concept that the peroxisomal export machinery may also participate in cargo release.[69] According to this idea, the ATP used by the REM to extract Ub-PEX5 from the DTM could also provide the energy necessary to disrupt the PEX5-cargo protein interaction, e.g., by

444 unfolding the PTS1-binding domain of PEX5. Further data are necessary to clarify these
445 important mechanistic aspects of the peroxisomal protein import machinery.

446 As it is well-known that the insertion of PEX5 into the peroxisomal membrane is a
447 cargo-dependent process,[69] the observation that both PEX5(L)$_{N526K}$–EGFP and PEX5(S)$_{\Delta C299}$-
448 PEX5L/PEX5R$_{\Delta N324}$-EGFP trigger peroxisome removal may be difficult to reconcile with the
449 suggested model that ubiquitinated versions of these proteins accumulate at the peroxisomal
450 membrane. However, here it is important to mention that (i) the N526K mutation in PEX5(L)
451 (and the corresponding N489K mutation in PEX5(S)) causes conformational alterations at the
452 N-terminal half of PEX5 mimicking the ones induced by binding of a PTS1-containing
453 peptide to the normal peroxin,[49] and (ii) also C-terminally truncated versions of PEX5 have
454 been reported to function as substrates for the peroxisomal DTM.[71] In this context, it is
455 interesting to mention that also PEX5(S)$_{N489K}$-EGFP, a version of PEX5 that lacks both its
456 PTS1 and PEX7-binding sites, can trigger peroxisome removal in SV40T-MEFs (data not
457 shown). Another intriguing observation is that non-tagged PEX5$_{C11S}$, but not PEX5$_{C11A}$,
458 triggered peroxisome removal in a small number of cells (**Fig. 4B**). Although PEX5$_{C11S}$ can
459 be monoubiquitinated at the DTM,[21] this process occurs at a very slow rate explaining why
460 this protein accumulates at the peroxisome. While further data are necessary to explain the
461 peroxisome removal phenotype induced by PEX5$_{C11S}$, it is tempting to speculate that PEX5
462 molecules retained for a long time at the peroxisomal membrane (e.g., in case the cargo
463 protein cannot be released from PEX5) become strongly (or even covalently) linked to some
464 DTM component(s) (e.g., by ROS-promoted mechanisms). In such a scenario, the subsequent
465 monoubiquitination of these molecules would trigger their REM-dependent extraction from
466 the DTM. However, this process would not be completed due to the strong PEX5-DTM
467 interaction, thus leading to the accumulation of partially exposed Ub-PEX5$_{C11S}$ species at the

peroxisome limiting membrane, similar to the ubiquitinatable PEX5-EGFP species used in this work.

As our data indicate that the addition of a bulky tag to the C terminus of PEX5 can result in the accumulation of partially extracted Ub-PEX5 on the peroxisomal surface, it is conceivable to envisage that this will eventually result in the recruitment of the autophagic machinery to the organelle. However, despite the fact that PEX5-mediated peroxisome removal depends on ATG5 and can be blocked by 3-MA and LY294002 (**Fig. 3**), we were repeatedly unable to colocalize peroxisomes with EGFP-MAP1LC3B, even when culturing the cells in medium supplemented with bafilomycin $A_1$ (**Fig. S20**) or chloroquine (data not shown). Nevertheless, here it should be mentioned that such colocalization could easily be observed upon expression of SLC25A17-Ub, even in the absence of autophagy inhibitors (**Fig. S20**, upper panels). In addition, unlike SLC25A17-Ub-, NBR1-, or PEX3-induced pexophagy, where peroxisomes cluster prior to degradation,[30,32,38] we did not observe any clustering of peroxisomes upon PEX5-KR expression (**Fig. S20**, compare the upper and lower panels). Note that this may also impede the likeliness of finding peroxisomes within autophagosomes, which have an approximate half-life of only 10 min.[44]

Regarding the observations that (i) the PEX5-EGFP-induced peroxisome removal phenotype in MEFs can be directly linked to the SV40 large T antigen-induced immortalization of these cells (data not shown), and (ii) SV40 large T antigen does not directly influence the expression levels of PEX5-EGFP (**Fig. S15**), it is important to note that SV40T-cells display cell type-specific global changes in gene expression (including some components of the cellular ubiquitination/deubiquitination machinery).[72,73] These observations suggest that the PEX5-EGFP-induced phenotype depends on a critical balance of multiple factors that remain to be determined and may even be cell type-specific (e.g., the promptness with which the Ub-moiety is recognized by the pexophagy machinery, the amount

493 of ubiquitin at the peroxisomal membrane, the kinetics of PEX5
494 ubiquitination/deubiquitination, and other potential quality control mechanisms, such as
495 proteasomal removal of [poly]ubiquitinated PEX5). For example, although PEX5
496 accumulates at the peroxisomal membrane in aging human fibroblasts, the number of
497 peroxisomes in these cells is profoundly increased.[74] However, here it is important to know
498 that (i) cellular aging is associated with an increase in the GSSG (oxidized glutathione)/GSH
499 (reduced glutathione) ratio,[75] and (ii) exposure of human PEX5 to GSSG results in a
500 ubiquitination-deficient PEX5 molecule.[76]

501 In conclusion, this work presents the first experimental evidence that addition of a
502 bulky tag to the C terminus of PEX5 interferes with the export of monoubiquitinated PEX5
503 from the DTM, and that this in turn can trigger peroxisome removal in SV40T-MEFs. These
504 findings strongly support the idea that peroxisome-associated monoubiquitinated PEX5 may
505 act as a key surveillance factor for the selective removal of dysfunctional peroxisomes in
506 mammalian cells.[30,39] In this context, we hypothesize that the bulky tag may mimic a cargo
507 protein that cannot be released from PEX5. However, as the study of mammalian pexophagy
508 is still in its infancy, this and many other intriguing questions remain. For example, like in
509 other studies that applied ectopic expression of ubiquitinated PMPs or PEX3 as a pexophagy
510 trigger,[30,32] PEX5-EGFP-induced pexophagy could only be partially blocked in conditions in
511 which macroautophagy was inhibited. Although this finding may suggest that some
512 peroxisomes can be removed by alternative degradation pathways,[77,78] this needs further
513 investigation. Also the potential involvement of the PEX5 export machinery, the specific
514 autophagy receptor proteins (e.g., SQSTM1, NBR1, OPTN, CALCOCO2, HDAC6, etc.), and
515 the mammalian Atg8 orthologs (i.e., the MAP1LC3 and GABARAP subfamilies)[79] need
516 further investigation. Indeed, as we currently cannot exclude the possibility that—upon
517 siRNA knockdown—the remaining amounts of PEX1, SQSTM1, or NBR1 are still sufficient

518 to sustain PEX5-EGFP-mediated peroxisome removal, the role of these proteins in this
519 process should ideally be studied in SV40T-knockout cell lines (and that are currently not
520 available). However, in case the triggering factor for peroxisome removal is not accumulation
521 of Ub-PEX5 at the DTM but rather accumulation of a partially dislocated Ub-PEX5 at the
522 DTM/REM, a complete inactivation of PEX1 would not result in an enhanced peroxisome
523 removal phenotype. Also, in the absence of a functional PEX5 export machinery, a ubiquitin-
524 dependent quality control pathway—called RADAR (receptor accumulation and degradation
525 in the absence of recycling)[80]—may be activated (assuming there is one in mammalian cells)
526 thereby leaving peroxisomes intact. Finally, it is also not yet clear why overexpression of
527 SLC25A17-Ub, NBR1, or PEX3 induces peroxisomal clustering,[30,32,38] whereas we do not
528 observe this phenotype during PEX5-EGFP-triggered pexophagy. Here it is tempting to
529 speculate that the clustering phenotype may represent a situation in which excessive
530 peroxisomes are massively removed, while the mechanism underlying PEX5-EGFP-induced
531 pexophagy may mimic a condition where dysfunctional organelles are individually degraded.
532 Also, given that SQSTM1 and NBR1 play a role in PMP-Ub- and PEX3-induced peroxisome
533 clustering and that this event precedes their targeting to autophagosomes and lysosomes,[30,32] it
534 may well be that SQSTM1 and/or NBR1 are not involved in PEX5-EGFP-induced
535 peroxisome removal.

536 In summary, this study provides strong evidence that monoubiquitinated PEX5 can
537 serve as a quality control mechanism to eliminate peroxisomes. In addition, it paves the way
538 for further investigations aimed at elucidating the molecular basis underlying peroxisome
539 degradation in mammalian cells, an essential prerequisite to understand how defects in this
540 process may be linked to clinically relevant disease phenotypes.

541 # Materials and methods

542 ***DNA manipulations and plasmids***

Polymerase chain reactions were routinely performed using *Pfx* DNA polymerase (Invitrogen, 11708039). Oligonucleotides and RNAi duplex oligonucleotides used in this study were synthesized by Integrated DNA Technologies and are listed in **Tables S1** and **S2,** respectively. The *Escherichia coli* strain *TOP10F'* (Invitrogen, C3030-03) was used for all DNA manipulations. Restriction enzymes were purchased from TaKaRa. The mammalian expression vectors pEGFP-N1, pCMV-Tag 2B, pKillerRed-dMito, and pHT2 were commercially obtained from Clontech (6085-1), Stratagene (211172), Evrogen (FP964), and Promega (G8241), respectively. A detailed description of the non-commercial plasmids used in this study is available in the supplementary information (**Materials S1**). All new plasmids were verified by DNA sequencing (LGC Genomics).

***Cell culture, immunofluorescence and live-cell microscopy***

SV40 large T-antigen transformed *Atg5*$^{+/+}$, *atg5*$^{-/-}$, and *Perk*$^{+/+}$ MEFs were kindly provided by Dr. P. Agostinis (KU Leuven, Belgium).[56,57] *PEX5*$^{-/-}$ human fibroblasts, spontaneously transformed *Sqstm1*$^{+/+}$ MEFs, and the murine oligodendrocyte cell line (158N) were generous gifts from Dr. G. Dodt (University of Tübingen, Germany), Dr. T. Yanagawa (Niigata University, Japan), and Dr. S. Ghandour (University of Strasbourg, France), respectively.[58,76,81] Control primary MEFs (C57BL/6) and rat embryonic fibroblasts (Sprague-Dawley) were generated as before.[76] All cells were cultured at 37°C in a humidified 5% $CO_2$ incubator in minimum essential medium Eagle α (Lonza, BE12-169F) supplemented with 10% (v/v) fetal bovine serum superior (Biochrom AG, BCHRS0615), 2 mM Ultraglutamine-1 (Lonza, BE17-605E/U1/12), and 0.2% (v/v) Mycozap (Lonza, VZA-2012). MEFs were transfected using Invitrogen´s Neon Transfection System (1350 V, 30 ms pulse width, 1 pulse).[82] To knock down the expression of target genes, the cells were first electroporated with the appropriate Dicer-substrate RNAs (DsiRNAs), and—2 d later—co-electroporated with the same DsiRNAs and the plasmid encoding the protein under study. The final

568 concentrations in the 10-µl microporator tip were 2 µM for individual DsiRNAs; 0.66 µM per
569 DsiRNA for TriFECTa RNAi kit duplex combinations, and 1 µg of plasmid. The transfected
570 cells were either processed for indirect immunofluorescence or lysed for SDS-PAGE and
571 immunoblot analysis (for sample analysis under nonreducing conditions, cell pellets were first
572 treated with 10 mM N-ethylmaleimide (NEM; Across Organics, 156100100) to block
573 deubiquitinases and any endogenous nucleophilic groups that may attack the Ub-PEX5-EGFP
574 thioester). Samples for immunofluorescence microscopy were fixed and processed as
575 described before.[47] The rabbit polyclonal antiserum against human PEX14,[83] the mouse
576 polyclonal antiserum against bovine CAT/catalase[84] and the antibodies raised against a
577 mixture of peroxisomal matrix proteins (ab-MF16)[85] have been described elsewhere. DAPI
578 (Roche, 10236276001), Hoechst 33258 (Sigma, 14530), the rabbit anti-ABCD3 antibodies
579 (Sigma, P0497), the mouse anti-FLAG antibodies (Stratagene, 200472-21), the rabbit anti-
580 HaloTag antibodies (Promega, G9281), the mouse anti-LAMP1 antibodies (BD Pharmingen,
581 553792), the rabbit (Cell Signaling Technology, 2775) and mouse (Nanotools, 0231-
582 100/LC3-5F10) anti-LC3B antibodies, the rabbit (Proteintech, 16004-1-AP) and mouse
583 (Abcam, ab55474) anti-NBR1 antibodies, the rabbit anti-PEX1 antibodies (Bio-Connect,
584 13669-1-AP), the rabbit anti-SQSTM1 antibodies (Sigma, P0067), the rabbit anti-ubiquitin
585 antibodies (Cell Signaling Technology, 3933), the mouse anti-mono/polyubiquitin
586 monoclonal antibody (Enzo, FK2, BML-PW8810), the Alexa Fluor 350- (Invitrogen,
587 A11069), Alexa Fluor 488- (Invitrogen, A11017 and A11070) or Texas Red- (TxRed;
588 Calbiochem, 401355 and 401230) conjugated secondary antibodies were commercially
589 obtained. To interfere with the autophagic process, the cells were cultivated in the presence of
590 10 mM 3-MA (Sigma, M9281), 100 nM bafilomycin $A_1$ (Sigma, B1793), 10 µM LY294002
591 (Sigma, L-9908), 20 µM chloroquine (Sigma, C6628), 10 µM E-64 (MP Biomedicals,
592 152846), 10 µM pepstatin A (Sigma, P-4265), and/or 100 µM leupeptin hemisulfate (Fluka,

62070). Cells for live-cell imaging were seeded and imaged in FluoroDish cell culture dishes (World Precision Instruments, FD35-100). Where indicated, cells were treated for 1 h with 500 nM MitoTracker® Red CM-$H_2$Xros (Life Technologies, M7513) or ER-Tracker™ Blue-White DPX (Life Technologies, E-12253) in regular cell culture medium, and washed once with the same medium immediately before imaging. The sequential labeling of live cells expressing HaloTag-HsHAO2 (hydroxyacid oxidase 2 [long chain]) was done for the specified period of time with 250 nM HaloTag TMR (Promega, G8251) and 10 nM HaloTag R110Direct (Promega, G3221) ligands as described elsewhere.[86] After the first and second labeling reactions, the cells were washed 6 times and once, respectively, with standard growth medium. Fluorescence was evaluated on a motorized inverted IX-81 microscope (Olympus), controlled by Cell-M software (Olympus) and equipped with a temperature-, humidity-, and $CO_2$-controlled incubation chamber. The technical specifications of the objectives, excitation and emission filters, and digital camera have been described elsewhere.[42] The Cell-M software was used for quantitative image analysis.

***In vitro import/export assays***

Rat liver postnuclear supernatant (PNS) for *in vitro* assays was prepared in SEM buffer (0.25 M sucrose, 20 mM MOPS-KOH, pH 7.2, 1 mM EDTA-NaOH, pH 7.2) supplemented with 2 μg/ml E-64 (Sigma, E3132), as described before.[70] [$^{35}$S]-labeled proteins were synthesized *in vitro* using the TNT® T7 Quick Coupled Transcription/Translation System (Promega, L1170) in the presence of [$^{35}$S]methionine (specific activity >1000 Ci/mmol; PerkinElmer Life Sciences, NEG709A001MC). In the *in vitro* import reactions (100 μl final volume), 1 μl of the relevant $^{35}$S-labeled protein was added to 600 μg of PNS protein that had been primed for import (incubation for 5 min at 37ºC in import buffer (0.25 M sucrose, 50 mM KCl, 20 mM MOPS-KOH, pH 7.2, 3 mM $MgCl_2$, 20 μM methionine, and 2 μg/ml E-64) containing 0.3 mM ATP (Sigma, A2383).[22,67] Import assays also contained 2

618 mM glutathione (Sigma, G4251), 3 µM ubiquitin aldehyde[53] and, where indicated, ATP (3
619 mM), AMP-PNP (3 mM; Sigma, A2647), bovine ubiquitin (15 µM; Sigma, U6253) or GST-
620 Ub[21] (15 µM). After incubation for 30 min at 37°C, samples were treated with 20 mM NEM
621 (Sigma, E3876) on ice for 5 min, as described before.[48] To separate organelles from soluble
622 proteins, the *in vitro* import reactions were diluted with ice-cold SEMK buffer (SEM buffer
623 containing 80 mM KCl) and centrifuged at 16,000 x *g* for 20 min at 4°C. Samples were
624 subjected to trichloroacetic acid precipitation and processed for SDS-PAGE under reducing or
625 nonreducing conditions, as specified. Protease protection assays were done using proteinase K
626 (400 µg/ml final concentration; Sigma, P2308) for 40 min on ice.[53] The 2-step *in vitro*
627 import/export assay was exactly done as described before.[68] For the immunoprecipitation
628 assays, protease-treated organelles from import assays were solubilized for 30 min at 4ºC in
629 immunoprecipitation buffer (50 mM Tris-HCl, pH 7.5, 150 mM NaCl, 1 mM EDTA-NaOH,
630 pH 8.0, 0.1% [w/v] SDS [Merck, 1137601000], 1% [w/v] Triton X-100 [Sigma, T9284],
631 0.5% [w/v] sodium deoxycholate [Sigma, D5670], 500 µg/ml phenylmethylsulfonyl fluoride
632 [Sigma, P7626] and 1/200 [v/v] mammalian protease inhibitor mixture [Sigma, P8346]). After
633 removing the insoluble material (15 min at 15,000 x *g*), the supernatant fraction was divided
634 in 3 aliquots. One aliquot (total) was kept at 4ºC during the complete procedure and then
635 subjected to trichloroacetic acid precipitation. The other 2 aliquots received 25 µl (bed
636 volume) of protein A-Sepharose® beads (Sigma, P3391) that were preincubated with either 3
637 µl of an anti-EGFP serum[88] or a control serum, and incubated for 2 h at 4ºC with gentle
638 shaking. After removing the supernatant fraction, the beads were washed 3 times with
639 immunoprecipitation buffer and once with 1X phosphate-buffered saline (137 mM NaCl, 2.7
640 mM KCl, 4.3 mM $Na_2HPO_4$, 1.1 mM $KH_2PO_4$). Immunoprecipitated proteins were eluted
641 with 45 µl of Laemmli sample buffer and the corresponding immunodepleted supernatant
642 fractions were subjected to trichloroacetic acid precipitation.

643 ***Statistical analysis***

644 Stastistics were performed on the VassarStats statistical computation website
645 (http://vassarstats.net/). A 2-sample t-Test for independent samples was used to analyze the
646 results. The significance levels were set at $p<0.05$ (denoted by *) and $p<0.01$ (denoted by **).

647 ## Acknowledgments

648 We thank Dr. P. Agostinis (KU Leuven, Belgium) for the SV40 large T antigen-
649 transformed *Atg5*$^{+/+}$, *atg5*$^{-/-}$, and *Perk*$^{+/+}$ MEFs, Dr. T. Yanagawa (Niigata University, Japan)
650 for the spontaneously transformed *Sqstm1*$^{+/+}$ MEFs, Dr. G. Dodt (University of Tübingen,
651 Germany) for the *PEX5*$^{-/-}$ human fibroblasts, and Dr. S. Ghandour (University of Strasbourg,
652 France) for the murine oligodendrocyte cell line. We are also grateful to Dr. M. Baes (KU
653 Leuven, Belgium), Dr. T. Yoshimori (National Institute of Genetics, Japan), Dr. T. Voets (KU
654 Leuven, Belgium), and Dr. S. M. Di Pietro (Colorado State University, CO, USA) for the
655 plasmids encoding myc-tagged MmPEX5(L), EGFP-MAP1LC3B, LAMP1-EGFP, or
656 LAMP2A-EGFP, respectively. This work was supported by grants from the 'Fonds voor
657 Wetenschappelijk Onderzoek-Vlaanderen (Onderzoeksprojecten G.0754.09 and G095315N)'
658 (to MF and PVV), the KU Leuven (OT/09/045, OT/14/100, and DBOF/10/059) (to MF and
659 PVV), and by FEDER funds through the Operational Competitiveness Programme –
660 COMPETE and by National Funds through FCT – Fundação para a Ciência e a Tecnologia
661 under the projects FCOMP-01-0124-FEDER-019731 (PTDC/BIA-BCM/118577/2010) and
662 FCOMP-01-0124-FEDER-022718 (PEst-C/SAU/LA0002/2011) (to JEA). MN was supported
663 by a FLOF fellowship from the Department of Cellular and Molecular Medicine (KU
664 Leuven). TF was supported by Fundação para a Ciência e a Tecnologia, Programa
665 Operacional Potencial Humano do QREN, and Fundo Social Europeu.

666 ## Conflict of interest

667 The authors declare no conflict of interest.

668

669 ## References


670 1. Mizushima N, Komatsu M. Autophagy: renovation of cells and tissues. Cell 2011; 147:
671 728-741.
672 2. Kaushik S, Cuervo AM. Chaperone-mediated autophagy: a unique way to enter the
673 lysosome world. Trends Cell Biol 2012; 22: 407-417.
674 3. Boya P, Reggiori F, Codogno P. Emerging regulation and functions of autophagy. Nat
675 Cell Biol 2013; 15: 713-720.
676 4. Mizushima N, Yoshimori T, Ohsumi Y. The role of Atg proteins in autophagosome
677 formation. Annu Rev Cell Dev Biol 2011; 27: 107-132.
678 5. Araki Y, Ku WC, Akioka M, May AI, Hayashi Y, Arisaka F, Ishihama Y, Ohsumi Y.
679 Atg38 is required for autophagy-specific phosphatidylinositol 3-kinase complex integrity.
680 J Cell Biol 2013; 203: 299-313.
681 6. Green DR, Levine B. To be or not to be? How selective autophagy and cell death govern
682 cell fate. Cell 2014; 157: 65-75.
683 7. Rogov V, Dötsch V, Johansen T, Kirkin V. Interactions between autophagy receptors and
684 ubiquitin-like proteins form the molecular basis for selective autophagy. Mol Cell 2014;
685 53: 167-178.
686 8. Van Veldhoven PP. Biochemistry and genetics of inherited disorders of peroxisomal fatty
687 acid metabolism. J Lipid Res 2010; 51: 2863-2895.
688 9. Braverman NE, Moser AB. Functions of plasmalogen lipids in health and disease.
689 Biochim Biophys Acta 2012; 1822: 1442-1452.
690 10. Islinger M, Grille S, Fahimi HD, Schrader M. The peroxisome: an update on mysteries.
691 Histochem Cell Biol 2012; 137: 547-574.

692 11. Fransen M, Nordgren M, Wang B, Apanasets O. Role of peroxisomes in ROS/RNS-
693 metabolism: implications for human disease. Biochim Biophys Acta 2012; 1822: 1363-
694 1373.
695 12. Forman HJ, Maiorino M, Ursini F. Signaling functions of reactive oxygen species.
696 Biochemistry 2010; 49: 835-842.
697 13. Sandalio LM, Rodríguez-Serrano M, Romero-Puertas MC, del Río LA. Role of
698 peroxisomes as a source of reactive oxygen species (ROS) signaling molecules. Subcell
699 Biochem 2013; 69: 231-255.
700 14. Nordgren M, Fransen M. Peroxisomal metabolism and oxidative stress. Biochimie 2014;
701 98: 56-62.
702 15. Brocard C, Hartig A. Peroxisome targeting signal 1: is it really a simple tripeptide?
703 Biochim Biophys Acta 2006; 1763: 1565-1573.
704 16. Fransen M. Peroxisome dynamics: molecular players, mechanisms, and (dys)functions.
705 ISRN Cell Biology 2012; Article ID 714192.
706 17. Gatto GJ Jr, Geisbrecht BV, Gould SJ, Berg JM. Peroxisomal targeting signal-1
707 recognition by the TPR domains of human PEX5. Nat Struct Biol 2000; 7: 1091-1095.
708 18. Braverman N, Dodt G, Gould SJ, Valle D. An isoform of Pex5p, the human PTS1
709 receptor, is required for the import of PTS2 proteins into peroxisomes. Hum Mol Genet
710 1998; 7: 1195-1205.
711 19. Francisco T, Rodrigues TA, Freitas MO, Grou CP, Carvalho AF, Sá-Miranda C, Pinto
712 MP, Azevedo JE. A cargo-centered perspective on the PEX5 receptor-mediated
713 peroxisomal protein import pathway. J Biol Chem 2013; 288: 29151-29159.
714 20. Platta HW, Hagen S, Reidick C, Erdmann R. The peroxisomal receptor dislocation
715 pathway: to the exportomer and beyond. Biochimie 2014; 98: 16-28.

716 21. Carvalho AF, Pinto MP, Grou CP, Alencastre IS, Fransen M, Sá-Miranda C, Azevedo JE.
717 Ubiquitination of mammalian Pex5p, the peroxisomal import receptor. J Biol Chem
718 2007; 282: 31267-31272.
719 22. Oliveira ME, Gouveia AM, Pinto RA, Sá-Miranda C, Azevedo JE. The energetics of
720 Pex5p-mediated peroxisomal protein import. J Biol Chem 2003; 278: 39483-39488.
721 23. Francisco T, Rodrigues TA, Pinto MP, Carvalho AF, Azevedo JE, Grou CP. Ubiquitin in
722 the peroxisomal protein import pathway. Biochimie 2014; 98: 29-35.
723 24. Platta HW, Hagen S, Erdmann R. The exportomer: the peroxisomal receptor export
724 machinery. Cell Mol Life Sci 2013; 70:1393-1411.
725 25. Shiozawa K, Maita N, Tomii K, Seto A, Goda N, Akiyama Y, Shimizu T, Shirakawa M,
726 Hiroaki H. Structure of the N-terminal domain of PEX1 AAA-ATPase. Characterization
727 of a putative adaptor-binding domain. J Biol Chem 2004; 279: 50060-50068.
728 26. Fujiki Y, Nashiro C, Miyata N, Tamura S, Okumoto K. New insights into dynamic and
729 functional assembly of the AAA peroxins, Pex1p and Pex6p, and their membrane
730 receptor Pex26p in shuttling of PTS1-receptor Pex5p during peroxisome biogenesis.
731 Biochim Biophys Acta 2012; 1823: 145-149.
732 27. Yokota S. Formation of autophagosomes during degradation of excess peroxisomes
733 induced by administration of dioctyl phthalate. Eur J Cell Biol 1993; 61: 67-80.
734 28. Iwata J, Ezaki J, Komatsu M, Yokota S, Ueno T, Tanida I, Chiba T, Tanaka K,
735 Kominami E. Excess peroxisomes are degraded by autophagic machinery in mammals. J
736 Biol Chem 2006; 281: 4035-4041.
737 29. Till A, Lakhani R, Burnett SF, Subramani S. Pexophagy: the selective degradation of
738 peroxisomes. Int J Cell Biol 2012; Article ID 512721.

739 30. Deosaran E, Larsen KB, Hua R, Sargent G, Wang Y, Kim S, Lamark T, Jauregui M, Law
740 K, Lippincott-Schwartz J, et al. NBR1 acts as an autophagy receptor for peroxisomes. J
741 Cell Sci 2013; 126: 939-952.
742 31. Nordgren M, Wang B, Apanasets O, Fransen M. Peroxisome degradation in mammals:
743 mechanisms of action, recent advances, and perspectives. Front Physiol 2013; Article ID
744 145.
745 32. Yamashita SI, Abe K, Tatemichi Y, Fujiki Y. The membrane peroxin PEX3 induces
746 peroxisome-ubiquitination-linked pexophagy. Autophagy 2014; 10: 1549-1564.
747 33. Kim I, Lemasters JJ. Mitophagy selectively degrades individual damaged mitochondria
748 after photoirradiation. Antioxid Redox Signal 2011; 14: 1919-1928.
749 34. Rubio N, Verrax J, Dewaele M, Verfaillie T, Johansen T, Piette J, Agostinis P.
750 p38(MAPK)-regulated induction of p62 and NBR1 after photodynamic therapy promotes
751 autophagic clearance of ubiquitin aggregates and reduces reactive oxygen species levels
752 by supporting Nrf2-antioxidant signaling. Free Radic Biol Med 2014; 67: 292-303.
753 35. Wang Y, Nartiss Y, Steipe B, McQuibban GA, Kim PK. ROS-induced mitochondrial
754 depolarization initiates PARK2/PARKIN-dependent mitochondrial degradation by
755 autophagy. Autophagy 2012; 8: 1462-1476.
756 36. van Zutphen T, Veenhuis M, van der Klei IJ. Damaged peroxisomes are subject to rapid
757 autophagic degradation in the yeast *Hansenula polymorpha*. Autophagy 2011; 7; 863-
758 872.
759 37. Shibata M, Oikawa K, Yoshimoto K, Kondo M, Mano S, Yamada K, Hayashi M,
760 Sakamoto W, Ohsumi Y, Nishimura M. Highly oxidized peroxisomes are selectively
761 degraded via autophagy in *Arabidopsis*. Plant Cell 2013; 25: 4967-4983.

762 38. Kim PK, Hailey DW, Mullen RT, Lippincott-Schwartz J. Ubiquitin signals autophagic
763 degradation of cytosolic proteins and peroxisomes. Proc Natl Acad Sci USA 2008; 105:
764 20567-20574.
765 39. Brown AI, Kim PK, Rutenberg AD. PEX5 and ubiquitin dynamics on mammalian
766 peroxisome membranes. PLoS Comput Biol 2014; Article ID e1003426.
767 40. Okumoto K, Noda H, Fujiki Y. Distinct modes of ubiquitination of peroxisome-targeting
768 signal type 1 (PTS1) receptor Pex5p regulate PTS1 protein import. J Biol Chem 2014;
769 289: 14089-14108.
770 41. Bulina ME, Lukyanov KA, Britanova OV, Onichtchouk D, Lukyanov S, Chudakov DM.
771 Chromophore-assisted light inactivation (CALI) using the phototoxic fluorescent protein
772 KillerRed. Nat Protoc 2006; 1: 947-953.
773 42. Nordgren M, Wang B, Apanasets O, Brees C, Veldhoven PP, Fransen M. Potential
774 limitations in the use of KillerRed for fluorescence microscopy. J Microsc 2012; 245:
775 229-235.
776 43. Wang Y, Shyy JY, Chien S. Fluorescence proteins, live-cell imaging, and
777 mechanobiology: seeing is believing. Annu Rev Biomed Eng 2008; 10: 1-38.
778 44. Mizushima N, Yamamoto A, Hatano M, Kobayashi Y, Kabeya Y, Suzuki K, Tokuhisa T,
779 Ohsumi Y, Yoshimori T. Dissection of autophagosome formation using Apg5-deficient
780 mouse embryonic stem cells. J Cell Biol 2001; 152: 657-668.
781 45. Klionsky DJ, Abdalla FC, Abeliovich H, Abraham RT, Acevedo-Arozena A, Adeli K,
782 Agholme L, Agnello M, Agostinis P, Aguirre-Ghiso JA, et al. Guidelines for the use and
783 interpretation of assays for monitoring autophagy. Autophagy 2012; 8: 445-544.
784 46. Woudenberg J, Rembacz KP, Hoekstra M, Pellicoro A, van den Heuvel FA, Heegsma J,
785 van Ijzendoorn SC, Holzinger A, Imanaka T, Moshage H, et al. Lipid rafts are essential
786 for peroxisome biogenesis in HepG2 cells. Hepatology 2010; 52: 623-633.

787 47. Huybrechts SJ, Van Veldhoven PP, Brees C, Mannaerts GP, Los GV, Fransen M.
788 Peroxisome dynamics in cultured mammalian cells. Traffic 2009; 10: 1722-1733.
789 48. Grou CP, Carvalho AF, Pinto MP, Huybrechts SJ, Sá-Miranda C, Fransen M, Azevedo
790 JE. Properties of the ubiquitin-Pex5p thiol ester conjugate. J Biol Chem 2009; 284:
791 10504-10513.
792 49. Carvalho AF, Grou CP, Pinto MP, Alencastre IS, Costa-Rodrigues J, Fransen M, Sá-
793 Miranda C, Azevedo JE. Functional characterization of two missense mutations in Pex5p
794 - C11S and N526K. Biochim Biophys Acta 2007; 1773: 1141-1148.
795 50. Wang X, Herr RA, Hansen TH. Ubiquitination of substrates by esterification. Traffic
796 2012; 13: 19-24.
797 51. Okumoto K, Misono S, Miyata N, Matsumoto Y, Mukai S, Fujiki Y. Cysteine
798 ubiquitination of PTS1 receptor Pex5p regulates Pex5p recycling. Traffic 2011; 12: 1067-
799 1083.
800 52. Amery L, Sano H, Mannaerts GP, Snider J, Van Looy J, Fransen M, Van Veldhoven PP.
801 Identification of PEX5-related novel peroxisome-targeting signal 1 (PTS1)-binding
802 proteins in mammals. Biochem J 2001; 357: 635-646.
803 53. Grou CP, Francisco T, Rodrigues TA, Freitas MO, Pinto MP, Carvalho AF, Domingues
804 P, Wood SA, Rodríguez-Borges JE, Sá-Miranda C, et al. Identification of ubiquitin-
805 specific protease 9X (USP9X) as a deubiquitinase acting on ubiquitin-peroxin 5 (PEX5)
806 thioester conjugate. J Biol Chem 2012; 287: 12815-12827.
807 54. Miyata N, Okumoto K, Mukai S, Noguchi M, Fujiki Y. AWP1/ZFAND6 functions in
808 Pex5 export by interacting with cys-monoubiquitinated Pex5 and Pex6 AAA ATPase.
809 Traffic 2012; 13: 168-183.

55. Ivashchenko O, Van Veldhoven PP, Brees C, Ho YS, Terlecky SR, Fransen M. Intraperoxisomal redox balance in mammalian cells: oxidative stress and interorganellar crosstalk. Mol Biol Cell 2011; 22: 1440-1451.
56. Hosokawa N, Hara Y, Mizushima N. Generation of cell lines with tetracycline-regulated autophagy and a role for autophagy in controlling cell size. FEBS Lett 2006; 580: 2623-2629.
57. Verfaillie T, Rubio N, Garg AD, Bultynck G, Rizzuto R, Decuypere JP, Piette J, Linehan C, Gupta S, Samali A, Agostinis P. PERK is required at the ER-mitochondrial contact sites to convey apoptosis after ROS-based ER stress. Cell Death Differ 2012; 19: 1880-1891.
58. Komatsu M, Waguri S, Koike M, Sou YS, Ueno T, Hara T, Mizushima N, Iwata J, Ezaki J, Murata S, et al. Homeostatic levels of p62 control cytoplasmic inclusion body formation in autophagy-deficient mice. Cell 2007; 131: 1149-1163.
59. Deegan S, Saveljeva S, Gorman AM, Samali A. Stress-induced self-cannibalism: on the regulation of autophagy by endoplasmic reticulum stress. Cell Mol Life Sci 2013; 70: 2425-2441.
60. Campello S, Strappazzon F, Cecconi F. Mitochondrial dismissal in mammals, from protein degradation to mitophagy. Biochim Biophys Acta 2014; 1837: 451-460.
61. Michaeli S, Galili G. Degradation of organelles or specific organelle components via selective autophagy in plant cells. Int J Mol Sci 2014; 15: 7624-7638.
62. Aksam EB, de Vries B, van der Klei IJ, Kiel JA. Preserving organelle vitality: peroxisomal quality control mechanisms in yeast. FEMS Yeast Res 2009; 9: 808-820.
63. Oku M, Sakai Y. Peroxisomes as dynamic organelles: autophagic degradation. FEBS J 2010; 277: 3289-3294.

64. Manjithaya R, Nazarko TY, Farré JC, Subramani S. Molecular mechanism and physiological role of pexophagy. FEBS Lett 2010; 584: 1367-1373.
65. Nuttall JM, Motley AM, Hettema EH. Deficiency of the exportomer components Pex1, Pex6, and Pex15 causes enhanced pexophagy in *Saccharomyces cerevisiae*. Autophagy 2014; 10: 835-845.
66. Tomko RJ, Funakoshi M, Schneider K, Wang J, Hochstrasser M. Heterohexameric ring arrangement of the eukaryotic proteasomal ATPases: implications for proteasome structure and assembly. Mol Cell 2010; 38: 393-403.
67. Alencastre IS, Rodrigues TA, Grou CP, Fransen M, Sá-Miranda C, Azevedo JE. Mapping the cargo protein membrane translocation step into the PEX5 cycling pathway. J Biol Chem 2009; 284: 27243-27251.
68. Rodrigues TA, Alencastre IS, Francisco T, Brites P, Fransen M, Grou CP, Azevedo JE. A PEX7-centered perspective on the peroxisomal targeting signal type 2-mediated protein import pathway. Mol Cell Biol 2014; 34: 2917-2928.
69. Grou CP, Carvalho AF, Pinto MP, Alencastre IS, Rodrigues TA, Freitas MO, Francisco T, Sá-Miranda C, Azevedo JE. The peroxisomal protein import machinery - a case report of transient ubiquitination with a new flavor. Cell Mol Life Sci 2009; 66: 254-262.
70. Gouveia AM, Guimarães CP, Oliveira ME, Reguenga C, Sá-Miranda C, Azevedo JE. Characterization of the peroxisomal cycling receptor, Pex5p, using a cell-free *in vitro* import system. J Biol Chem 2003; 278: 226-232.
71. Gouveia AM, Guimarães CP, Oliveira ME, Sá-Miranda C, Azevedo JE. Insertion of Pex5p into the peroxisomal membrane is cargo protein-dependent. J Biol Chem 2003; 278: 4389-4392.

857 72. Cantalupo PG, Sáenz-Robles MT, Rathi AV, Beerman RW, Patterson WH, Whitehead
858 RH, Pipas JM. Cell-type specific regulation of gene expression by simian virus 40 T
859 antigens. Virology 2009; 386: 183-191.
860 73. Rathi AV, Sáenz Robles MT, Cantalupo PG, Whitehead RH, Pipas JM. Simian virus 40
861 T-antigen-mediated gene regulation in enterocytes is controlled primarily by the Rb-E2F
862 pathway. J Virol 2009; 83: 9521-9531.
863 74. Legakis JE, Koepke JI, Jedeszko C, Barlaskar F, Terlecky LJ, Edwards HJ, Walton PA,
864 Terlecky SR. Peroxisome senescence in human fibroblasts. Mol Biol Cell 2002; 13:
865 4243-4255.
866 75. Muller M. Cellular senescence: molecular mechanisms, *in vivo* significance, and redox
867 considerations. Antioxid Redox Signal 2009; 11: 59-98.
868 76. Apanasets O, Grou CP, Van Veldhoven PP, Brees C, Wang B, Nordgren M, Dodt G,
869 Azevedo JE, Fransen M. PEX5, the shuttling import receptor for peroxisomal matrix
870 proteins, is a redox-sensitive protein. Traffic 2014; 15: 94-103.
871 77. Yokota S, Oda T, Fahimi HD. The role of 15-lipoxygenase in disruption of the
872 peroxisomal membrane and in programmed degradation of peroxisomes in normal rat
873 liver. J Histochem Cytochem 2001; 49: 613-622.
874 78. Juenemann K, Reits EA. Alternative macroautophagic pathways. Int J Cell Biol 2012;
875 2012: Article ID 189794.
876 79. Shaid S, Brandts CH, Serve H, Dikic I. Ubiquitination and selective autophagy. Cell
877 Death Differ 2013; 20: 21-30.
878 80. Léon S1, Subramani S. A conserved cysteine residue of *Pichia pastoris* Pex20p is
879 essential for its recycling from the peroxisome to the cytosol. J Biol Chem 2007; 282:
880 7424-7430.

881 81. Feutz AC, Pham-Dinh D, Allinquant B, Miehe M, Ghandour MS. An immortalized jimpy
882 oligodendrocyte cell line: defects in cell cycle and cAMP pathway. Glia 2001; 34: 241-
883 252.
884 82. Brees C, Fransen M. A cost-effective approach to microporate mammalian cells with the
885 Neon Transfection System. Anal Biochem 2014; 466: 49-50.
886 83. Amery L, Fransen M, De Nys K, Mannaerts GP, Van Veldhoven PP. Mitochondrial and
887 peroxisomal targeting of 2-methylacyl-CoA racemase in humans. J Lipid Res 2000; 41:
888 1752-1759.
889 84. Huybrechts SJ, Van Veldhoven PP, Hoffman I, Zeevaert R, de Vos R, Demaerel P,
890 Brams M, Jaeken J, Fransen M, Cassiman D. Identification of a novel PEX14 mutation in
891 Zellweger syndrome. J Med Genet 2008; 45: 376-383.
892 85. Fransen M, Van Veldhoven PP, Subramani S. Identification of peroxisomal proteins by
893 using M13 phage protein VI phage display: molecular evidence that mammalian
894 peroxisomes contain a 2,4-dienoyl-CoA reductase. Biochem J 1999; 340: 561-568.
895 86. Fransen M. HaloTag as a tool to investigate peroxisome dynamics in cultured
896 mammalian cells. Methods Mol Biol 2014; 1174: 157-170.
897 87. Wilkinson KD, Gan-Erdene T, Kolli N. Derivitization of the C-terminus of ubiquitin and
898 ubiquitin-like proteins using intein chemistry: methods and uses. Methods Enzymol
899 2005; 399: 37-51.
900 88. Fransen M, Vastiau I, Brees C, Brys V, Mannaerts GP, Van Veldhoven PP. Potential role
901 for Pex19p in assembly of PTS-receptor docking complexes. J Biol Chem 2004; 279:
902 12615-12624.
903

## Figure legends

**Figure 1.** Expression of PEX5-KR triggers the removal of peroxisomes. SV40T-MEFs were transfected with plasmids encoding either **(A)** PEX5(L)-KR, **(B)** PEX5(L), or **(C)** KR. One day later, the cells were fixed, counterstained with DAPI, and processed for immunofluorescence with anti-PEX5 and/or anti-PEX14 antibodies followed by TxRed- and/or Alexa Fluor 488-conjugated secondary antibodies. **(A)** Upper and lower panels show a transfected cell where all, or most, peroxisomes are absent, respectively. Arrows indicate some of the remaining peroxisomes. Scale bar: 10 μm.

**Figure 2.** Expression of PEX5 proteins fused to a bulky C-terminal tag promotes a decrease in peroxisome number. SV40T-MEFs were cotransfected with plasmids encoding mitochondria-targeted EGFP (mt-EGFP; green color; marker for transfected cells) and either HsPEX5(S), HsPEX5(S)-FLAG, EGFP-HsPEX5(S), HsPEX5(S)-EGFP, HsPEX5(L), HsPEX5(L)-EGFP, HsPEX5(L)-KR, or mouse (*Mus musculus*, Mm) PEX5(L)-EGFP. One day later, the cells were fixed, counterstained with DAPI, and processed for immunofluorescence with anti-ABCD3 antibodies followed by TxRed- or Alexa Fluor 488-conjugated secondary antibodies. The number of peroxisomes in each transfected cell was counted and catalogued as more than 50 (>50), between 1 and 50 (1-50), or none (0). **(A)** Images of cells co-expressing mt-EGFP and PEX5(S)-EGFP with >50 (left panels), 1-50 (middle panels), or 0 (right panels) remaining peroxisomes are shown (these images depict representative examples of all phenotypes observed). Scale bar: 10 μm. **(B)** The percentage of transfected cells displaying each phenotype is plotted. The values above each bar represent the number of transfected cells analyzed per condition. A compilation of the results of at least 3 independent experiments (see **Fig S21**) is shown. The ">50 peroxisomes" values from the

927 "HsPEX5(S)" and "HsPEX5(L)" subpanels were statistically compared with the value from
928 the corresponding control (-) condition (* $p<0.05$; ** $p<0.01$).

929 **Figure 3.** PEX5-EGFP-induced peroxisome removal is dependent on autophagy. Control
930 (*CT*), *Atg5*$^{+/+}$ or *atg5*$^{-/-}$ SV40T-MEFs were co-transfected with plasmids encoding
931 mitochondria-targeted EGFP (marker for transfected cells) and a plasmid encoding either
932 PEX5-EGFP or FLAG-SLC25A17-Ub in the absence (-) or presence of 10 mM 3-
933 methyladenine (3-MA) or 10 μM LY294002 (LY). One day later, the cells were fixed and
934 processed for immunofluorescence with either anti-ABCD3 or anti-PEX14 antibodies.
935 Peroxisome degradation was quantified and plotted as in Figure 2B. The values above each
936 bar represent the number of transfected cells analyzed per condition. (**A, B**) A compilation of
937 the results of at least 3 independent experiments (see **Fig S22**) is shown. The ">50
938 peroxisomes" values from the different (sub)panels were statistically compared with the value
939 from the corresponding control condition (**, $p<0.01$). (**C**) The results of a single experiment
940 are shown.

941 **Figure 4.** The N-terminal cysteine residue that marks PEX5 for recycling is crucial for PEX5-
942 EGFP-induced pexophagy. SV40T-MEFs were cotransfected with plasmids encoding
943 mitochondria-targeted EGFP (marker for transfected cells) and either **(A)** full-length
944 PEX5(S)-EGFP (FL), PEX5(S)$_{\Delta N16}$-EGFP (ΔN16), or PEX5(S)$_{\Delta N110}$-EGFP (ΔN110), **(B)**
945 PEX5(L) (FL), PEX5(L)$_{C11K}$ (C11K), PEX5(L)$_{C11S}$ (C11S), or PEX5(L)$_{C11A}$ (C11A), with or
946 without a C-terminally fused EGFP-tag, or **(C)** PEX5(L)-EGFP (FL) PEX5(L)$_{K527R}$-EGFP
947 (K527R), PEX5(L)$_{N526K}$-EGFP (N526K), or PEX5(S)$_{\Delta C299}$-PEX5(L)/PEX5R$_{\Delta N326}$-EGFP
948 (SWAP). For clarity reasons, the PEX5(L)-EGFP data are presented in panels (**B and C**). One
949 day later, the cells were fixed and processed for immunofluorescence with anti-ABCD3
950 antibodies. Peroxisome degradation was quantified and plotted as in Figure 2B. The values

above each bar represent the number of transfected cells analyzed per condition. A compilation of the results of at least 3 independent experiments (see **Fig S23**) is shown. The ">50 peroxisomes" values from the (sub)panels were statistically compared with the value from the corresponding control (FL) condition (* $p<0.05$; ** $p<0.01$).

**Figure 5.** PEX5-EGFP is monoubiquitinated in a conserved cysteine-dependent manner but its ATP-dependent export is compromised. **(A)** Radiolabeled PEX5(L), PEX5(L)-EGFP, PEX5(L)$_{C11A}$-EGFP and PEX5(L)$_{C11S}$-EGFP were added to *in vitro* import assays in the presence of Ub aldehyde and either ATP (lanes 2 and 3) or AMP-PNP (lanes 4 and 5). After incubation at 37°C for 30 min, reactions were treated with NEM and centrifuged to obtain an organelle pellet (P) and a supernatant (S) fraction. One sixth of both fractions from each reaction (equivalent to 100 μg of PNS protein) was subjected to SDS-PAGE under nonreducing conditions and analyzed by autoradiography (an SDS-PAGE analysis of the same samples but under reducing conditions is shown in Fig. S12). *a* indicates modified (i.e., monoubiquitinated; see below) PEX5(L) or PEX5(L)-EGFP species. Lane I, 5% of the radiolabeled protein used in the assays. **(B)** Radiolabeled PEX5(L) and PEX5(L)-EGFP were incubated for 20 min at 37ºC with a postnuclear supernatant in import buffer supplemented with AMP-PNP. Import reactions were then centrifuged to separate the supernatant (Si) fraction from organelles (Pi). Isolated organelles were subsequently resuspended in an ATP-containing buffer, incubated for 5 min at 37ºC, and again centrifuged to separate the suspension into an organelle pellet (Pe) and supernatant (Se) fraction. Samples were separated under nonreducing conditions by SDS-PAGE and blotted onto a nitrocellulose membrane. The membrane was exposed to an x-ray film and afterwards probed with an antibody against ABCD3, a peroxisomal membrane protein. *a* indicates modified (i.e., monoubiquitinated; see below) PEX5(L) or PEX5(L)-EGFP species, respectively. Si, equivalent to 50 μg of PNS protein; Pi, Pe, and Se, equivalent to 250 μg of PNS protein. Lanes I1 and I2, 10% of the

radiolabeled proteins used in the assay. (**C**) Import assays made in the presence of GST-Ub show that the modified PEX5(L) species correspond to monoubiquitinated forms. PEX5(L) and PEX5(L)-EGFP were subjected to *in vitro* import reactions containing 3 mM AMP-PNP in the presence of either Ub or GST-Ub. After incubation, NEM was added and the organelles were isolated by centrifugation and analyzed by SDS-PAGE/autoradiography under reducing (+ DTT) or nonreducing (- DTT) conditions. *a* and *b* represent PEX5(L)/PEX5(L)-EGFP species containing one Ub and one GST-Ub, respectively. Lanes $I_1$ and $I_2$, 5% of the radiolabeled protein used in the assay. Numbers to the left indicate molecular masses of protein standards (in kDa).

**Figure 6.** Monoubiquitinated PEX5-EGFP trapped at the DTM in the presence of ATP is only partially protease protected. Radiolabeled PEX5(L), PEX5(L)-EGFP and PEX5(L)$_{C11A}$-EGFP were subjected to *in vitro* import assays in the presence of Ub aldehyde and either ATP or AMP-PNP, as indicated. After incubation at 37ºC, organelle suspensions were treated with proteinase K. NEM-treated organelles were then isolated, and subjected to SDS-PAGE under reducing (+ DTT) and non-reducing (- DTT) conditions. The autoradiographs (upper panels) and a section of the corresponding Ponceau S-stained membranes (lower panels) are shown. *a* and *b* represent DTM-inserted PEX5(L) exposing 2 kDa of its N terminus to the cytosol and DTM-embedded monoubiquitinated PEX5(L), respectively.[21] The asterisks mark a set of PEX5(L)-EGFP-derived fragments that are protease resistant. Lanes $I_1$, $I_2$, $I_3$, 5% of the radiolabeled protein used in the assays.

**Figure 7.** Downregulation of PEX1, SQSTM1, or NBR1 does not influence PEX5-EGFP-induced peroxisome removal. SV40T-MEFs were sequentially transfected with scrambled (NC1), PEX1-, SQSTM-, or NBR1-specific duplex siRNAs (DS) in combination or not with plasmids encoding mitochondria-targeted EGFP (marker for transfected cells) and **(A, C)**

HsPEX5-EGFP or **(B)** HsPEX5 (for details, see Materials and Methods). One day later, the cells were fixed and processed for immunofluorescence microscopy with anti-PEX14 antibodies. Peroxisome degradation was quantified and plotted as in Fig. 2B. The values above each bar represent the number of transfected cells analyzed per condition. A compilation of the results of at least 2 independent experiments (see **Fig. S24**) is shown. The ">50 peroxisomes" values from the (sub)panels were statistically compared with the value from the corresponding control (NC1) condition and found not to be statistically different.

## Supplementary Figure legends

**Figure S1.** PEX5-EGFP-induced peroxisome removal is not affected by expression of mitochondria-targeted EGFP. SV40T-MEFs were transfected with plasmids encoding HsPEX5(S)-EGFP (5S-EGFP) or HsPEX5(L)-EGFP (5L-EGFP) in combination (+) or not (-) with a plasmid encoding mitochondria-targeted EGFP (mt-EGFP). One day later, the cells were fixed and processed for immunofluorescence microscopy. The number of peroxisomes per transfected cell was quantified in each condition and plotted as in Figure 2B. The values above each bar represent the number of transfected cells analyzed per condition. The results are a compilation of at least 3 independent experiments. The ">50 peroxisomes" values from the "+" and "-" conditions were statistically compared and found not to be statistically significant.

**Figure S2.** Expression of PEX5-EGFP triggers the degradation of both peroxisomal membrane and matrix proteins. SV40T-MEFs were transfected with a plasmid encoding PEX5(L)-EGFP. One day later, the cells were fixed, counterstained with DAPI, and processed for immunofluorescence microscopy with antibodies raised against PEX14, ABCD3, CAT/catalase, or a mixture of peroxisomal matrix proteins (ab-MF16). Representative images are shown. Scale bar: 10 μm.

**Figure S3.** PEX5-EGFP-induced peroxisome removal depends on the amount of input DNA. SV40T-MEFs were transiently transfected with a plasmid (1 µg/electroporation) encoding mitochondria-targeted EGFP (marker for transfected cells) in combination or not with increasing concentrations of a plasmid encoding PEX5(L)-EGFP. One day later, the cells were fixed and processed for immunofluorescence microscopy with anti-ABCD3 antibodies. In each condition, the number of peroxisomes was quantified in 100 randomly selected transfected cells and plotted as in Figure 2B. The values are derived from a single experiment.

**Figure S4.** Kinetics of the PEX5-EGFP-induced decrease in peroxisome number. SV40T-MEFs were cotransfected with plasmids encoding PEX5(S)-EGFP and mitochondria-targeted EGFP (marker for transfected cells). The cells were fixed at the indicated time-points post-transfection and processed for immunofluorescence microscopy with anti-ABCD3 antibodies. Peroxisome degradation was quantified as in Figure 2B, and the resulting values were plotted as (**A**) percentages of transfected cells, or (**B**) percentages of transfected cells without peroxisomes (PO). The values in (**A**) are derived from one representative experiment. (**B**) N, number of independent experiments.

**Figure S5.** Large monomeric tags fused to the C terminus of PEX5 trigger the removal of peroxisomes in MEFs. SV40T-MEFs were transfected with a plasmid encoding PEX5(L)-HaloTag (PEX5(L)-HT) or PEX5(L)-mCherry. One day later, the cells were fixed, counterstained with DAPI, and processed for immunofluorescence microscopy with antibodies raised against HaloTag or PEX14. Representative images are shown. Scale bar: 10 µm.

**Figure S6.** The basal turnover rates of peroxisomes in MEFs are not high enough to consider a reduction in peroxisome formation as the causal factor for the PEX5-EGFP-induced phenotype. SV40T-MEFs, transiently transfected with a plasmid encoding HaloTag-HsHAO2

(H-PTS1), were sequentially incubated with the red-fluorescent HaloTag TMR (TMR) ligand (4-22 h post-transfection) and the green fluorescent HaloTag R110Direct (R110) ligand (31-48 h post-transfection; this condition was included to visualize transfected cells in case the basal turnover rates of peroxisomes would be very high). The cells were subjected to live-cell imaging at 24 and 48 h post-transfection. (**A**) Schematic overview of the procedure. (**B**) Representative staining patterns of cells expressing H-PTS1. Scale bar: 10 μm. (**C**) The number of TMR-positive peroxisomes in each transfected cell was counted and catalogued as more than 50 (>50), between 1 and 50 (1-50), or none (0).

**Figure S7.** Number of peroxisomes in SV40T-MEFs. (**A**) Control (*CT*) and (**B**) *Atg5*$^{+/+}$ or *atg5*$^{-/-}$ SV40T-MEFs were transiently transfected with a plasmid encoding mitochondria-targeted EGFP (marker for transfected cells) in combination or not (-) with a plasmid encoding PEX5(L)-EGFP (5-EGFP). One day later, the cells were fixed and processed for immunofluorescence microscopy with anti-ABCD3 antibodies. In each condition, the number of peroxisomes was counted in randomly selected transfected cells. The results are presented as box-plot diagrams. The bottom and top of each box represent the 25$^{th}$ and 75$^{th}$ percentile values, respectively; the horizontal line inside each box depicts the median; and the horizontal lines below and above each box denote the mean minus and plus the standard deviation, respectively. The number of cells analyzed per condition is indicated above each measurement. The data were statistically compared: statistically significant differences ($p<0.01$) between cells from the same cell line expressing or not PEX5(L)-EGFP are indicated with an asterisk (*); significant differences ($p<0.01$) between identical conditions in different cell lines are marked with an alpha symbol (α). The results from a single experiment are shown.

**Figure S8.** Expression of PEX5-EGFP does not increase the levels of LC3-II in the absence or presence of bafilomycin $A_1$. SV40T-MEFs were either not transfected (-) or co-transfected with a plasmid encoding EGFP-MAP1LC3 (GFP-LC3) and PEX5(L)$_{C11A}$-EGFP or PEX5(L)-EGFP. Eight h later, the cells were incubated (+) or not (-) with 100 nM of bafilomycin $A_1$. Two h later, whole cell lysates were processed for SDS-PAGE, Ponceau S staining (to visualize total protein), and immunoblotting with antibodies against MAP1LC3B (LC3). The migration points of relevant molecular mass markers (expressed in kDa) are shown on the left. The arrowheads mark nonspecific protein bands. The numbers between brackets indicate the transfection efficiencies.

**Figure S9.** PEX5-EGFP expression does not affect the normal distribution and morphology of mitochondria and the ER. SV40T-MEFs were transfected with a plasmid encoding PEX5(S)-EGFP. One day later the cells were treated with either (upper panels) MitoTracker® Red CM-$H_2$Xros (MitoTracker) or (lower panels) ER-Tracker™ Blue-White DPX (ER-Tracker; recolored in red) to visualize the mitochondria and the ER, respectively. Representative images are shown. Scale bar: 10 μm.

**Figure S10.** EGFP-tagged PEX5 proteins partially localize to peroxisomes. SV40T-MEFs were transfected with plasmids encoding either PEX5(S)-EGFP (upper panels), PEX5(L)$_{C11S}$-EGFP (middle panels), or PEX5(L)$_{C11A}$-EGFP (lower panels). One day later, the cells were fixed, counterstained with DAPI, and processed for immunofluorescence microscopy with anti-ABCD3 antibodies followed by TxRed-conjugated secondary antibodies. Scale bar: 10 μm.

**Figure S11.** PEX5-EGFP, PEX5$_{C11A}$-EGFP, and PEX5$_{C11S}$-EGFP are expressed at similar levels. SV40T-MEFs were transfected with a plasmid encoding mitochondria-targeted EGFP (marker for transfected cells) in combination or not (-) with PEX5(L)-EGFP (WT),

PEX5(L)$_{C11A}$-EGFP (C11A), or PEX5(L)$_{C11S}$-EGFP (C11S). One day later, whole cell lysates were subjected to SDS-PAGE and processed for immunoblotting. (**A**) Anti-EGFP (upper part) and anti-ACTB/β-actin (lower part) staining patterns. The migration points of relevant molecular mass markers (expressed in kDa) are shown on the right. (**B**) The anti-EGFP signals were quantified and normalized to ACTB. Note that (i) the transfection efficiencies were similar (30-37%) for all conditions, and (ii) the level of pexophagy induction by each PEX5-EGFP variant was comparable to that shown in Fig. 4B (data not shown). The results from a single experiment are shown.

**Figure S12**. Reducing SDS-PAGE analysis of the *in vitro* import reactions performed with radiolabeled PEX5(L), PEX5(L)-EGFP, PEX5(L)$_{C11A}$-EGFP and PEX5(L)$_{C11S}$-EGFP. Fractions from the *in vitro* assays shown in Fig. 5A (one sixth of each fraction) were subjected to SDS-PAGE under reducing conditions. An autoradiograph is shown. Numbers to the left indicate molecular masses of protein standards (in kDa).

**Figure S13.** The organelle-associated protease-resistant domains of Ub-PEX5(L)-EGFP represent C-terminal fragments of PEX5(L) including EGFP. Radiolabeled PEX5(L)-EGFP was subjected to an *in vitro* import reaction in the presence of ATP. After protease treatment, the organelles were isolated and solubilized with immunoprecipitation buffer. The clarified supernatant (Total), the immunoprecipitates (IP) obtained using either an anti-EGFP (GFP) or control serum (Ctrl), and the corresponding immunodepleted supernatant fractions (ID) were analyzed by SDS-PAGE/autoradiography. Numbers to the left indicate the molecular masses of protein standards (in kDa). F, front.

**Figure S14.** PEX5-EGFP is posttranslationally modified in a conserved cysteine-dependent manner upon expression in MEFs. SV40T-MEFs were either not transfected (-) or transfected with a plasmid encoding PEX5$_{C11A}$-EGFP (C11A) or PEX5-EGFP (WT). One day later,

whole cell lysates were subjected to SDS-PAGE under nonreducing (- DTT) or reducing (+ DTT) conditions and processed for immunoblotting with antibodies against PEX5. Arrows and arrowheads mark PEX5-specific and -nonspecific bands, respectively. The migration points of relevant molecular mass markers (expressed in kDa) are shown on the left.

**Figure S15.** SV40 large T antigen does not affect the expression levels of pEGFP-N1-encoded proteins in MEFs. Spontaneously- (S) or SV40 large T antigen (SVT)-transformed MEFs were either not transfected (-) or transfected with a plasmid encoding PEX5(L)-EGFP (5-EGFP) or mitochondria-targeted EGFP (mt-EGFP). One day later, whole cell lysates were subjected to SDS-PAGE and processed for immunoblotting with antibodies against EGFP. The migration points of relevant molecular mass markers (expressed in kDa) are shown on the left. Note that mt-EGFP contains 2 mitochondrial targeting signals arranged in tandem and that the arrows in the lower panel mark the differentially cleaved isoforms of this protein. The numbers between brackets indicate the transfection efficiencies.

**Figure S16.** Ability of different PEX5 proteins to complement or inhibit peroxisomal matrix protein import. SV40T-*PEX5*$^{-/-}$ human fibroblasts (*PEX5*$^{-/-}$ SV40T-HuFs) or spontaneously transformed *Sqstm1*$^{+/+}$ mouse embryonic fibroblasts (MEFs) were transfected with a plasmid encoding peroxisomal mCherry (mCherry-PTS1) together or not (-) with a plasmid encoding either wild-type HsPEX5(L) (WT), HsPEX5(L)$_{C11K}$ (C11K), HsPEX5(L)$_{C11S}$ (C11S), HsPEX5(L)$_{C11A}$ (C11A), or HsPEX5(L)-EGFP (GFP). The subcellular distribution pattern of mCherry-PTS1 was analyzed at the indicated days post-transfection (dpt): PO, peroxisomal; PO/C, mixed peroxisomal-cytosolic; and C, cytosolic. Representative images of the observed patterns are shown for each cell type (scale bar: 10 μm). (**A**) Complementation activity of PEX5 variants in *PEX5*$^{-/-}$ SV40T-HuFs. The results are plotted as percentage-based stacked bar charts (n = 100). (**B**) Inhibitory activity of PEX5 variants on peroxisomal matrix protein

import in *Sqstm1*$^{+/+}$ MEFs. The results are plotted as percentage-based stacked bar charts (n = 150).

**Figure S17.** Efficiency of DsiRNA delivery. SV40T-MEFs were sequentially transfected with a non-fluorescently- (DS NC1) or fluorescently-labeled (DS TYE 563) scrambled control RNA duplex (for details, see Materials and Methods). Six h after the second transfection, the nuclei were stained with Hoechst 33258 and the cells were processed for live-cell imaging. Representative images are shown. Scale bar: 50 μm.

**Figure S18.** Effect of downregulation of PEX1 on PTS1 protein import. SV40T-MEFs were sequentially transfected with scrambled (DS NC1) or PEX1-specific duplex siRNAs (DS PEX1) in combination or not with a plasmid encoding peroxisome-targeted EGFP (EGFP-PTS1) (for details, see Materials and Methods). One day later, the cells were (**A**) fixed and processed for immunofluorescence microscopy with antibodies against PEX1 or PEX14 (scale bar: 10 μm), (**B**) processed for immunoblotting with antibodies against PEX1 (the migration point of a relevant molecular mass marker (expressed in kDa) is shown on the right; the asterisk indicates a nonspecific protein band recognized by the anti-PEX1 antibody), or (**C**) analyzed by live-cell imaging to determine the subcellular distribution pattern of EGFP-PTS1 (PO, peroxisomal; PO/C, mixed peroxisomal-cytosolic; and C, cytosolic; the results are plotted as percentage-based stacked bar charts; n > 450).

**Figure S19.** Downregulation of SQSTM1 and NBR1 in SV40T-MEFs. SV40T-MEFs were sequentially transfected with scrambled (NC1) or SQSTM1- or NBR1-specific duplex siRNAs (DS) in combination or not with a plasmid encoding PEX5-EGFP (for details, see Materials and Methods). One day later, the cells were (**A, B**) fixed and processed for immunofluorescence microscopy with antibodies against SQSTM1, NBR1 or PEX14 (scale bar: 10 μm), or (**C, D**) first incubated (+) or not (-) with 100 nM bafilomycin $A_1$ (baf $A_1$) for 3

h and subsequently processed for immunoblotting with antibodies against SQSTM1 or NBR1. The migration points of relevant molecular mass markers (expressed in kDa) are shown on the left. The asterisk marks a degradation product of SQSTM1, and the arrowheads mark nonspecific protein bands.

**Figure S20.** Peroxisomes do not cluster or colocalize with EGFP-MAP1LC3B during PEX5-mediated pexophagy. SV40T-MEFs were cotransfected with plasmids encoding EGFP-MAP1LC3B and either FLAG-SLC25A17-Ub (upper panels) or PEX5(L)-KR (lower panels) in the presence (lower panels) or not (upper panels) of 100 nM bafilomycin $A_1$. 12 h later, the cells were fixed and processed for immunofluorescence microscopy with anti-FLAG and/or anti-ABCD3 antibodies followed by TxRed- and/or Alexa Fluor 350-conjugated secondary antibodies. Representative images are shown. Scale bar: 10 μm.

**Figure S21.** Expression of PEX5 proteins fused to a bulky C-terminal tag promotes a decrease in peroxisome number. SV40T-MEFs were cotransfected with plasmids encoding mitochondria-targeted EGFP (marker for transfected cells) and either (**A**) HsPEX5(S), (**B**) HsPEX5(S)-FLAG, (**C**) EGFP-HsPEX5(S), (**D**) HsPEX5(S)-EGFP, (**E**) HsPEX5(L), (**F**) HsPEX5(L)-EGFP, (**G**) HsPEX5(L)-KR, or (**H**) MmPEX5(L)-EGFP. One day later, the cells were fixed, counterstained with DAPI, and processed for immunofluorescence microscopy with anti-ABCD3 antibodies followed by TxRed- or Alexa Fluor 488-conjugated secondary antibodies. The number of peroxisomes in each transfected cell was counted and catalogued as more than 50 (>50), between 1 and 50 (1-50), or none (0). The average percentage of transfected cells displaying each phenotype is plotted. The error bars represent the standard deviations. N, number of independent experiments.

**Figure S22.** PEX5-EGFP-induced peroxisome removal is dependent on autophagy. (**A**) *Atg5*$^{+/+}$, (**B**) *atg5*$^{-/-}$ or (**C-E**) control (*CT*) SV40T-MEFs were cotransfected with plasmids

encoding mitochondria-targeted EGFP (marker for transfected cells) and a plasmid encoding PEX5-EGFP in the absence (**A-C**) or presence (**D**) of 10 mM 3-methyladenine (3-MA) or (**E**) 10 μM LY294002 (LY). One day later, the cells were fixed and processed for immunofluorescence microscopy with either anti-ABCD3 or anti-PEX14 antibodies. The number of peroxisomes in each transfected cell was quantified and plotted as in Figure S21. The error bars represent the standard deviations. N, number of independent experiments.

**Figure S23.** The N-terminal cysteine residue that marks PEX5 for recycling is crucial for PEX5-EGFP-induced pexophagy. SV40T-MEFs were cotransfected with plasmids encoding mitochondria-targeted EGFP (marker for transfected cells) and either (**A**) HsPEX5(S)-EGFP, (**B**) HsPEX5(S)$_{\Delta N16}$-EGFP, (**C**) HsPEX5(S)$_{\Delta N110}$-EGFP, (**D**) HsPEX5(L), (**E**) HsPEX5(L)$_{C11S}$, (**F**) HsPEX5(L)$_{C11A}$, (**G**) HsPEX5(L)-EGFP, (**H**) HsPEX5(L)$_{C11S}$-EGFP, (**I**) HsPEX5(L)$_{C11A}$-EGFP, (**J**) HsPEX5(L)$_{C11K}$-EGFP, (**K**) PEX5(L)$_{K527R}$-EGFP, (**L**) PEX5(L)$_{N526K}$-EGFP, or (**M**) PEX5(S)$_{\Delta C299}$-PEX5L/PEX5R$_{\Delta N326}$-EGFP (HsPEX5(S)$_{SWAP}$-EGFP). One day later, the cells were fixed and processed for immunofluorescence microscopy with anti-ABCD3 antibodies followed by TxRed-conjugated secondary antibodies. The number of peroxisomes in each transfected cell was quantified and plotted as in Figure S21. The error bars represent the standard deviations. N, number of independent experiments.

**Figure S24.** Downregulation of SQSTM1, NBR1, or PEX1 does not influence PEX5-EGFP-induced peroxisome removal. SV40T-MEFs were sequentially transfected with scrambled (NC1), SQSTM-, NBR1-, or PEX1-specific duplex siRNAs (DS) in combination or not with plasmids encoding mitochondria-targeted EGFP (marker for transfected cells) and HsPEX5-EGFP (for details, see Materials and Methods). One day later, the cells were fixed and processed for immunofluorescence microscopy with anti-PEX14 antibodies followed by TxRed-conjugated secondary antibodies. The number of peroxisomes in each transfected cell

1215 was quantified and plotted as in Figure S21. The error bars represent the standard deviations.

1216 N, number of independent experiments.

Figure S1

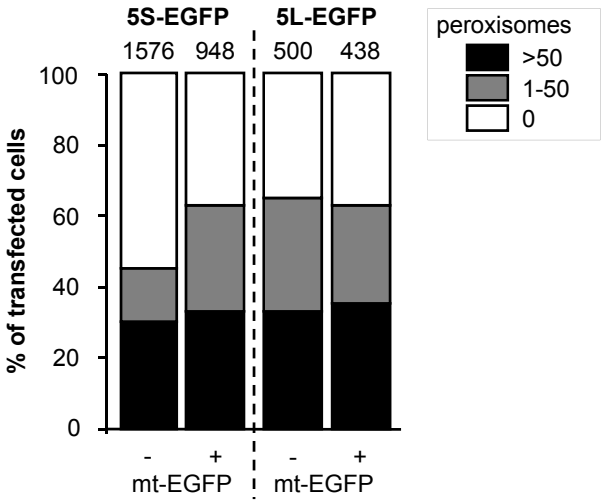
5S-EGFP
5L-EGFP
1576
948
500
438
peroxisomes
>50
1-50
0
% of transfected cells
100
80
60
40
20
0
-
+
-
+
mt-EGFP
mt-EGFP

Figure S2

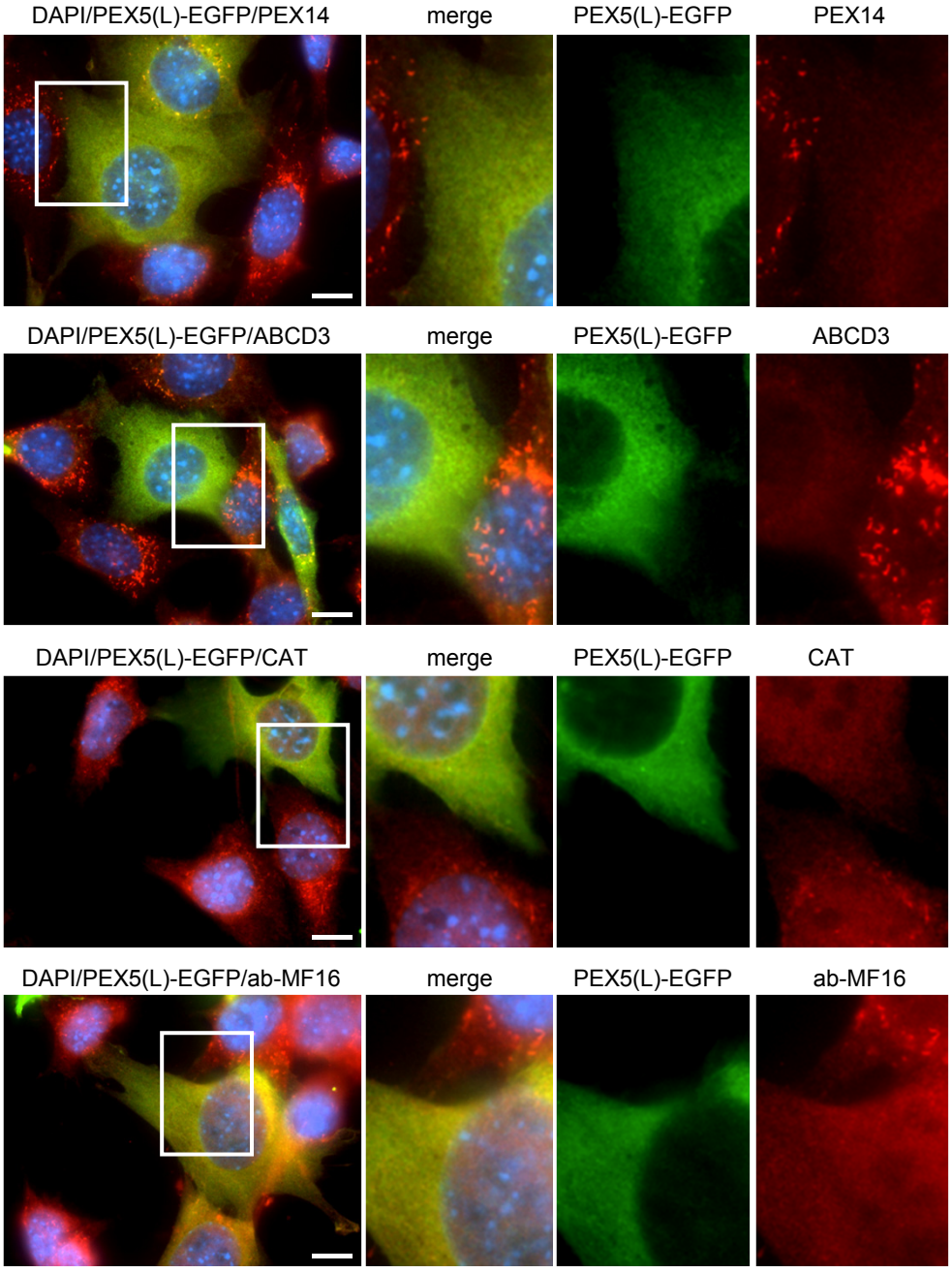
DAPI/PEX5(L)-EGFP/PEX14
merge
PEX5(L)-EGFP
PEX14
DAPI/PEX5(L)-EGFP/ABCD3
merge
PEX5(L)-EGFP
ABCD3
DAPI/PEX5(L)-EGFP/CAT
merge
PEX5(L)-EGFP
CAT
DAPI/PEX5(L)-EGFP/ab-MF16
merge
PEX5(L)-EGFP
ab-MF16

Figure S3

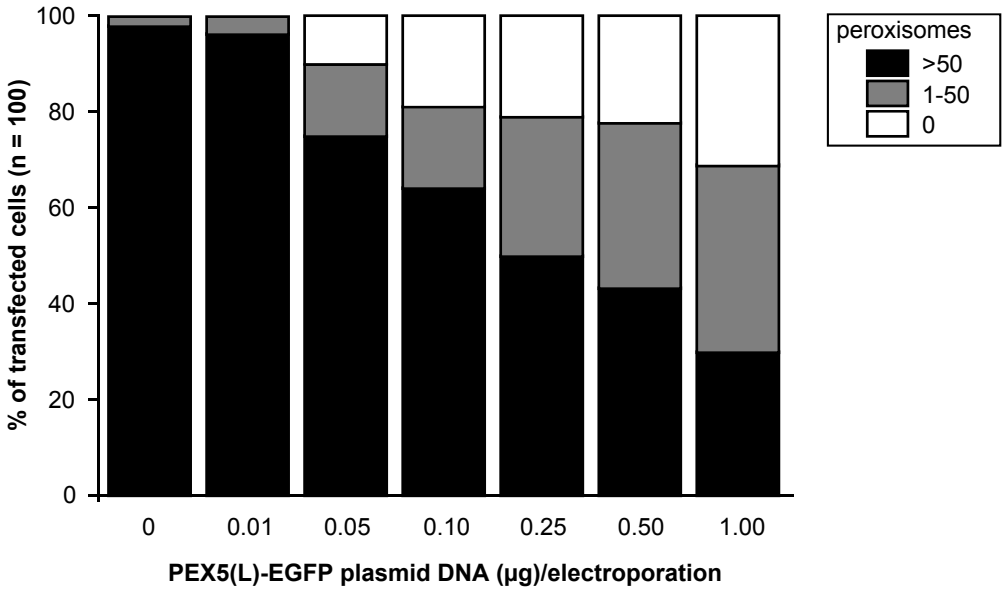
100
80
60
40
20
0
% of transfected cells (n = 100)
0
0.01
0.05
0.10
0.25
0.50
1.00
PEX5(L)-EGFP plasmid DNA (µg)/electroporation
peroxisomes
>50
1-50
0

Figure S4

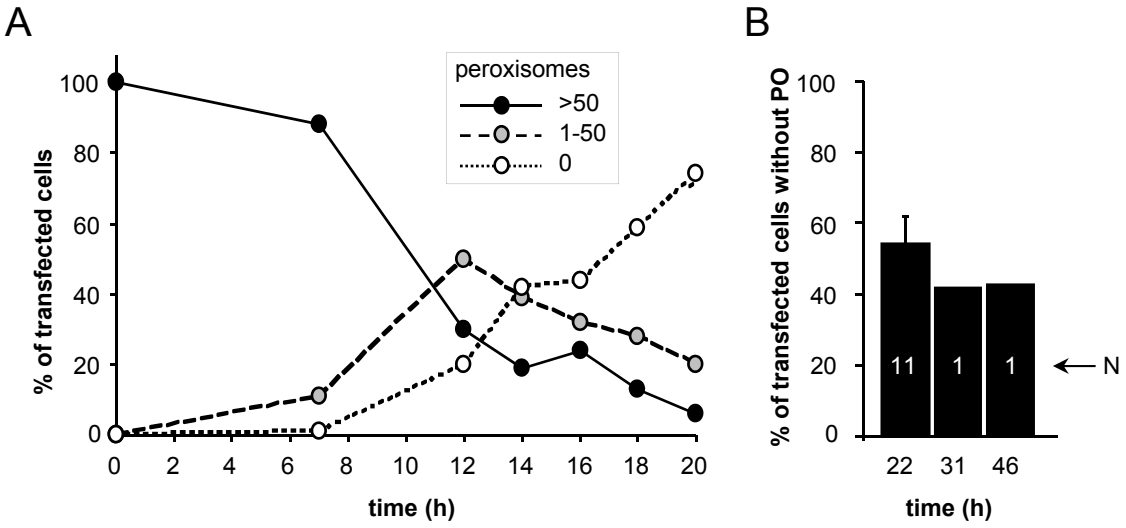
A
peroxisomes
>50
1-50
0
% of transfected cells
time (h)
B
% of transfected cells without PO
11
1
1
N
time (h)

Figure S5

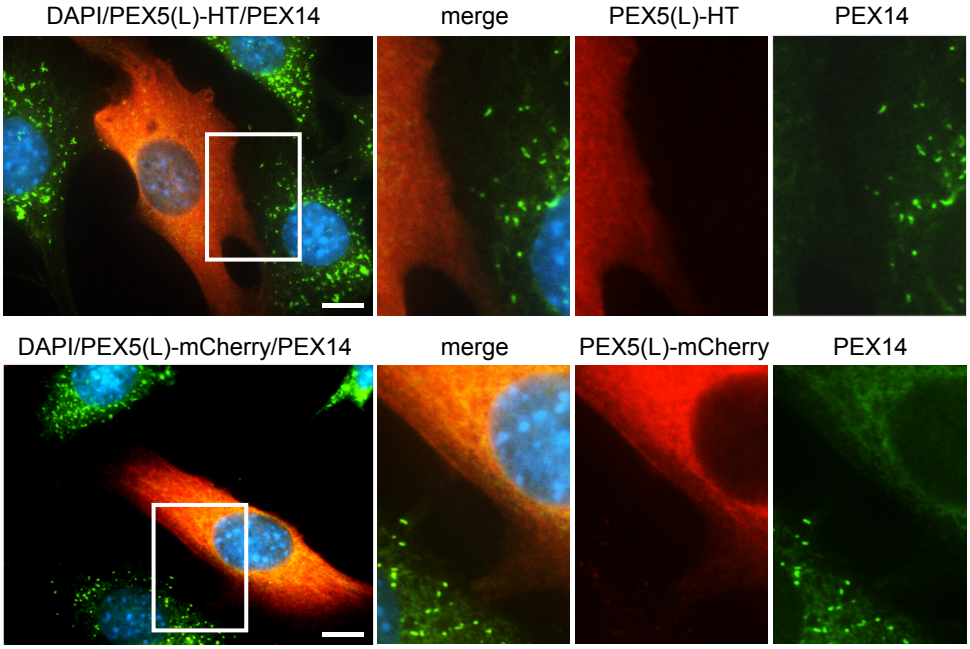
DAPI/PEX5(L)-HT/PEX14
merge
PEX5(L)-HT
PEX14
DAPI/PEX5(L)-mCherry/PEX14
merge
PEX5(L)-mCherry
PEX14

Figure S6

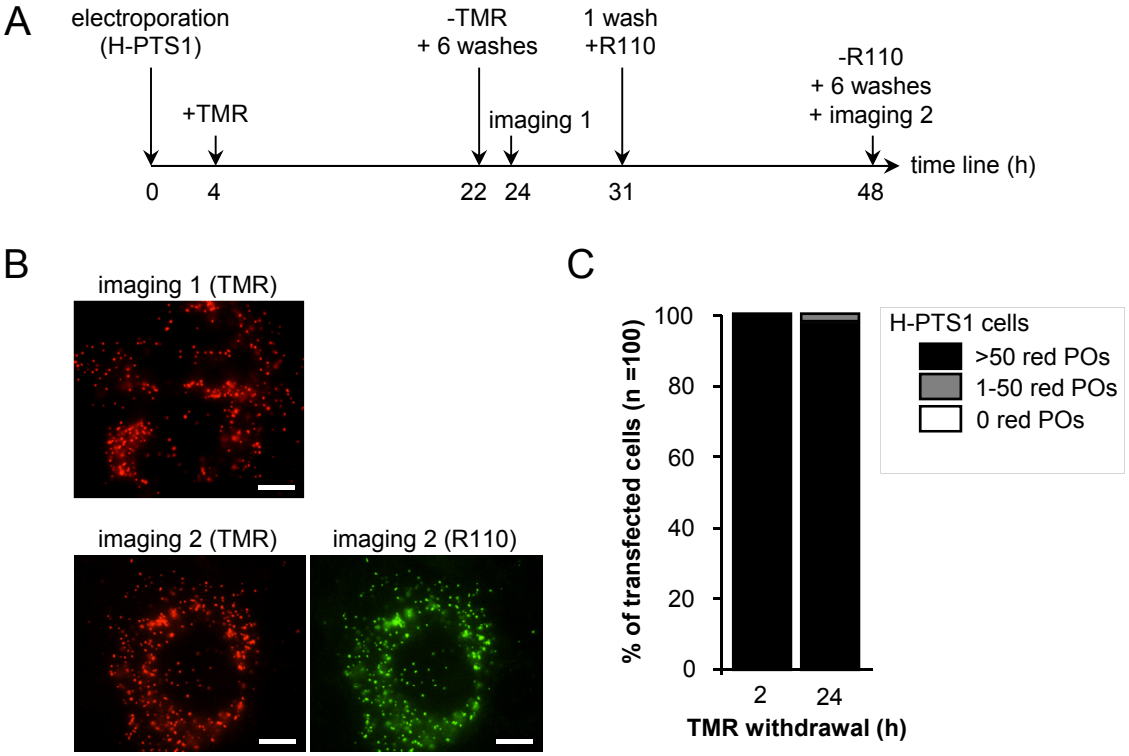
A
electroporation
(H-PTS1)
+TMR
-TMR
+ 6 washes
imaging 1
1 wash
+R110
-R110
+ 6 washes
+ imaging 2
time line (h)
0
4
22
24
31
48
B
imaging 1 (TMR)
imaging 2 (TMR)
imaging 2 (R110)
C
% of transfected cells (n =100)
100
80
60
40
20
0
2
24
TMR withdrawal (h)
H-PTS1 cells
>50 red POs
1-50 red POs
0 red POs

Figure S7

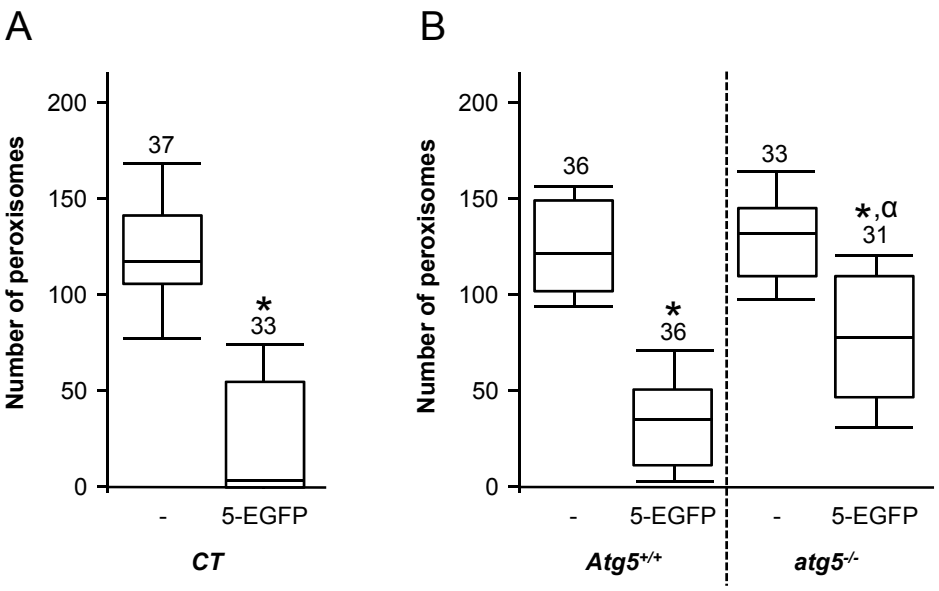
A
B
Number of peroxisomes
200
150
100
50
0
37
33
*
-
5-EGFP
CT
36
36
33
31
*,α
Atg5+/+
atg5-/-

Figure S8

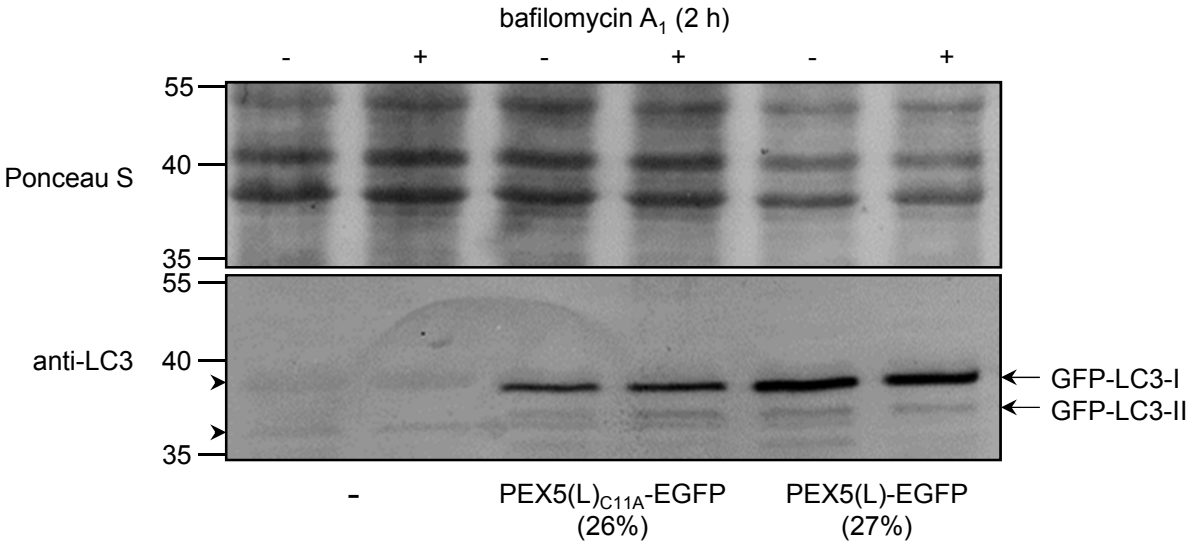
bafilomycin A1 (2 h)
- + - + - +
55
40
35
Ponceau S
55
40
35
anti-LC3
GFP-LC3-I
GFP-LC3-II
-
PEX5(L)C11A-EGFP
(26%)
PEX5(L)-EGFP
(27%)

Figure S9

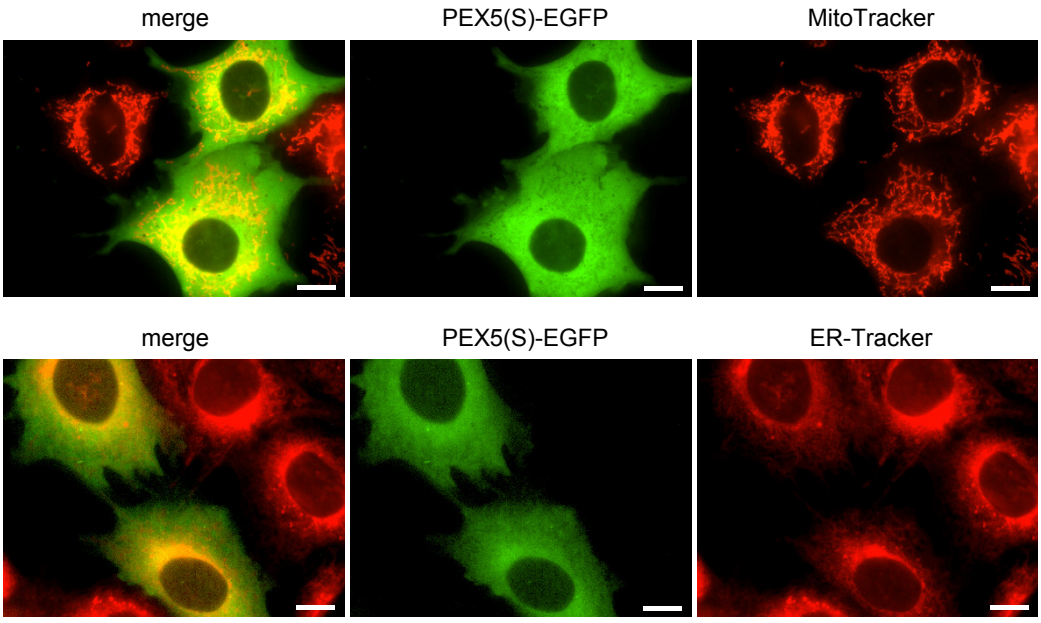

Figure S10

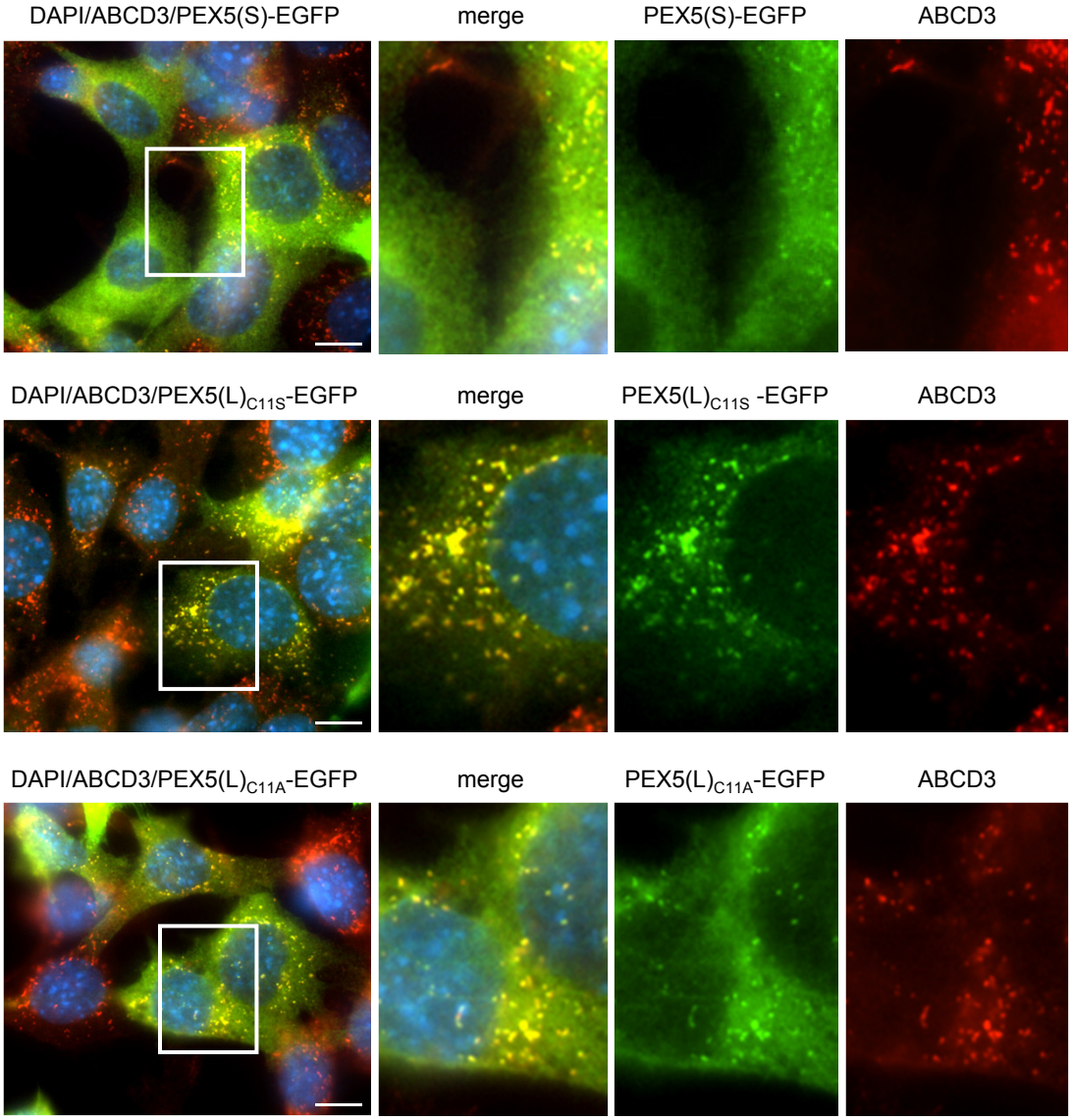
DAPI/ABCD3/PEX5(S)-EGFP
merge
PEX5(S)-EGFP
ABCD3
DAPI/ABCD3/PEX5(L)C11S-EGFP
merge
PEX5(L)C11S -EGFP
ABCD3
DAPI/ABCD3/PEX5(L)C11A-EGFP
merge
PEX5(L)C11A-EGFP
ABCD3

Figure S11

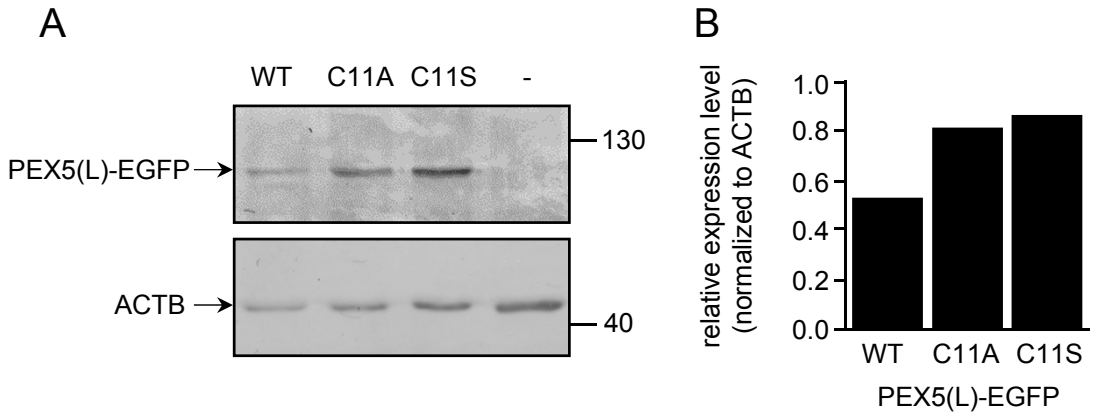
A
WT
C11A
C11S
-
PEX5(L)-EGFP
ACTB
130
40
B
relative expression level
(normalized to ACTB)
1.0
0.8
0.6
0.4
0.2
0.0
WT
C11A
C11S
PEX5(L)-EGFP

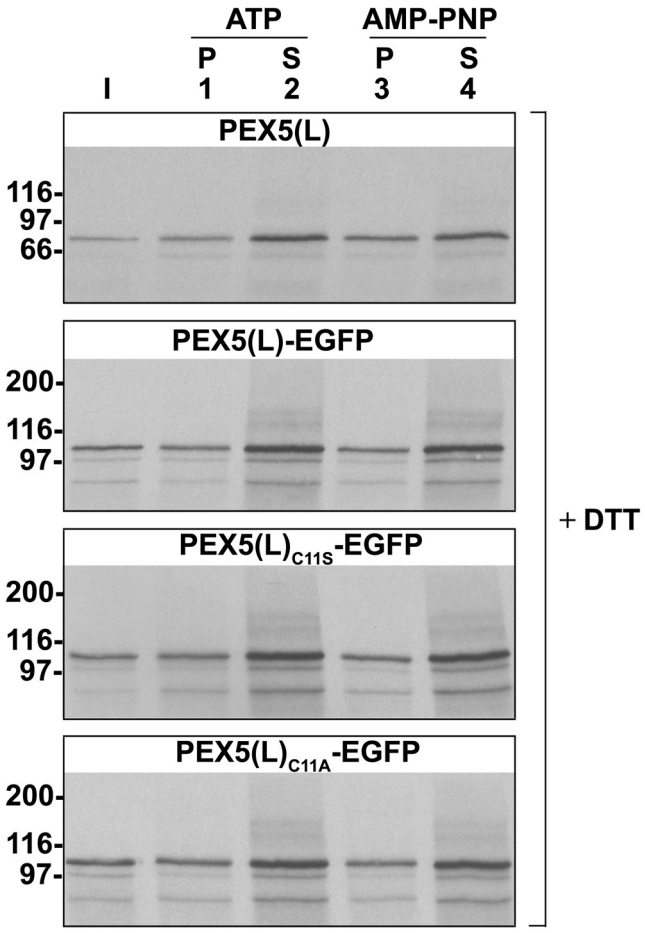
ATP
AMP-PNP
P
S
P
S
I
1
2
3
4
PEX5(L)
116-
97-
66-
PEX5(L)-EGFP
200-
116-
97-
PEX5(L)C11S-EGFP
200-
116-
97-
PEX5(L)C11A-EGFP
200-
116-
97-
+ DTT

**Figure S12**

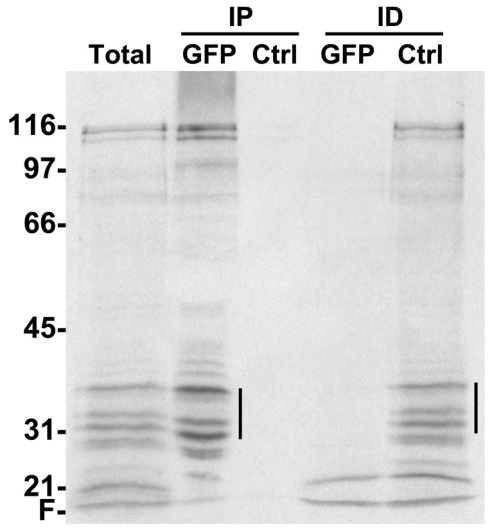


**Figure S13**

Figure S14

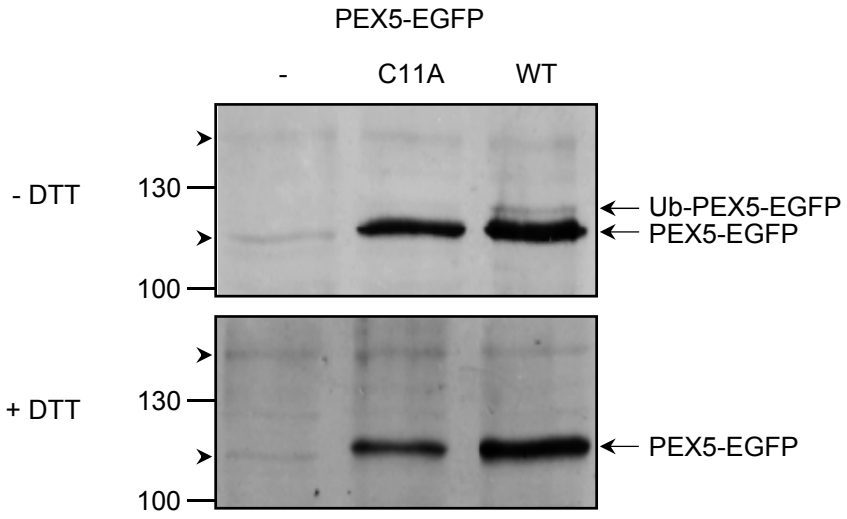
PEX5-EGFP
-
C11A
WT
- DTT
130
100
Ub-PEX5-EGFP
PEX5-EGFP
+ DTT
130
100
PEX5-EGFP

Figure S15

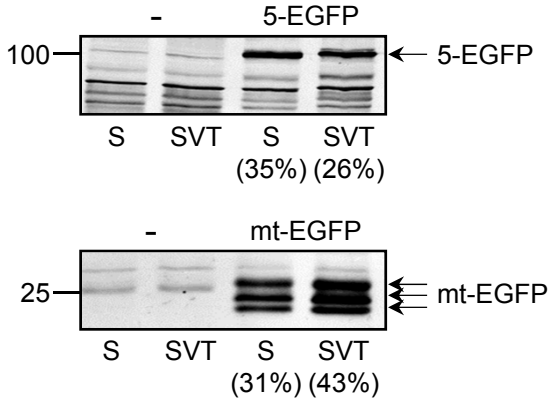
-
5-EGFP
100
5-EGFP
S
SVT
S
SVT
(35%)
(26%)
-
mt-EGFP
25
mt-EGFP
S
SVT
S
SVT
(31%)
(43%)

Figure S16

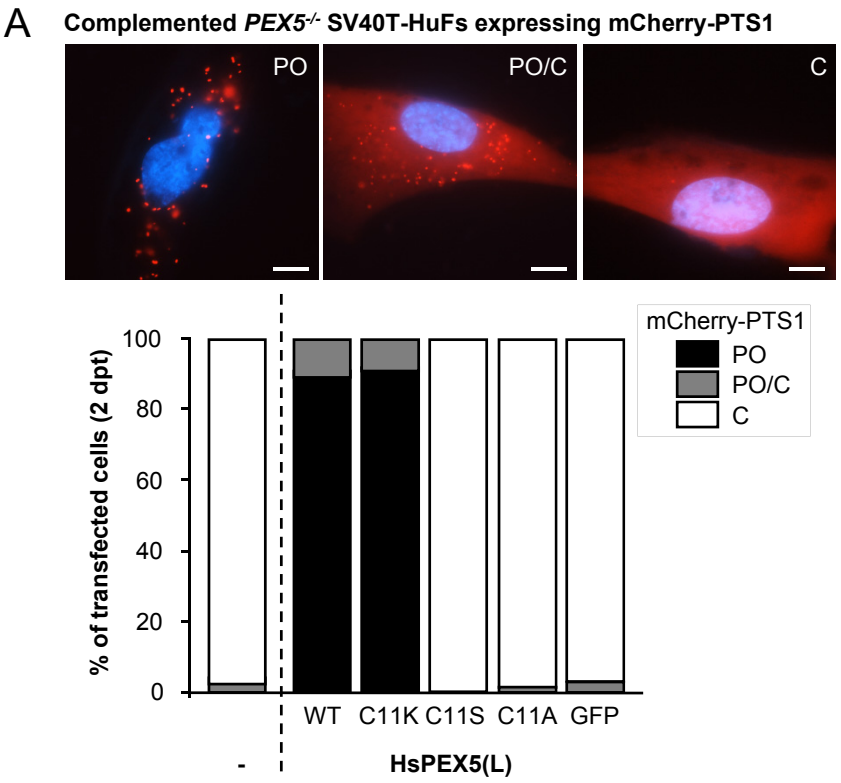
A
Complemented PEX5-/- SV40T-HuFs expressing mCherry-PTS1
PO
PO/C
C
% of transfected cells (2 dpt)
100
80
60
40
20
0
mCherry-PTS1
PO
PO/C
C
WT
C11K
C11S
C11A
GFP
-
HsPEX5(L)

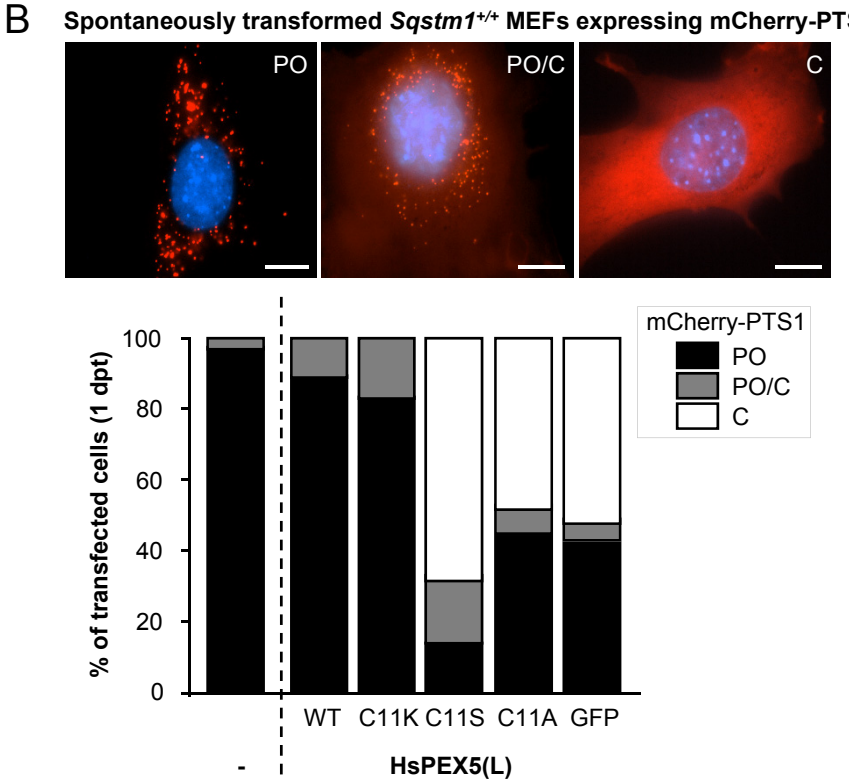
B
Spontaneously transformed Sqstm1+/+ MEFs expressing mCherry-PTS1
PO
PO/C
C
% of transfected cells (1 dpt)
100
80
60
40
20
0
mCherry-PTS1
PO
PO/C
C
WT
C11K
C11S
C11A
GFP
-
HsPEX5(L)

Figure S17

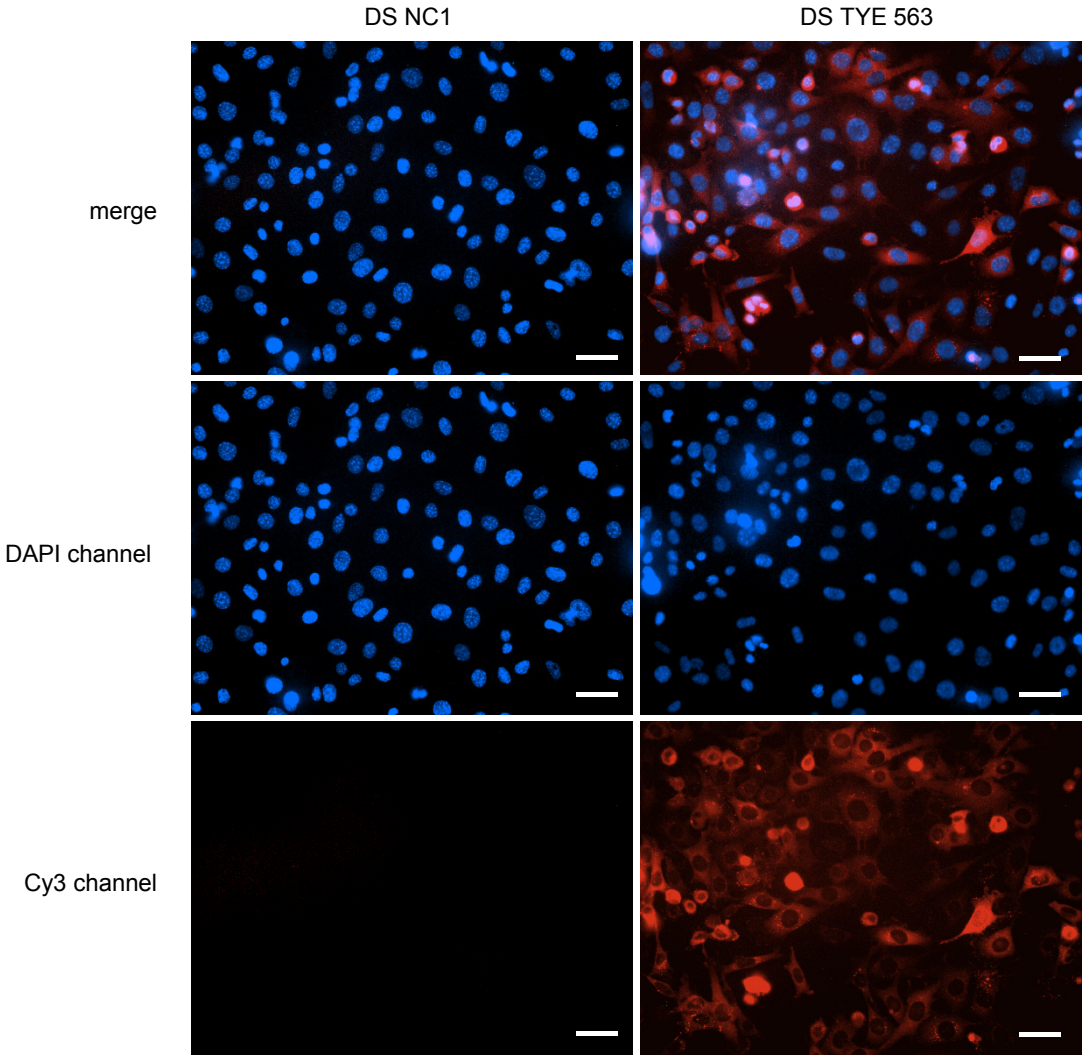

Figure S18

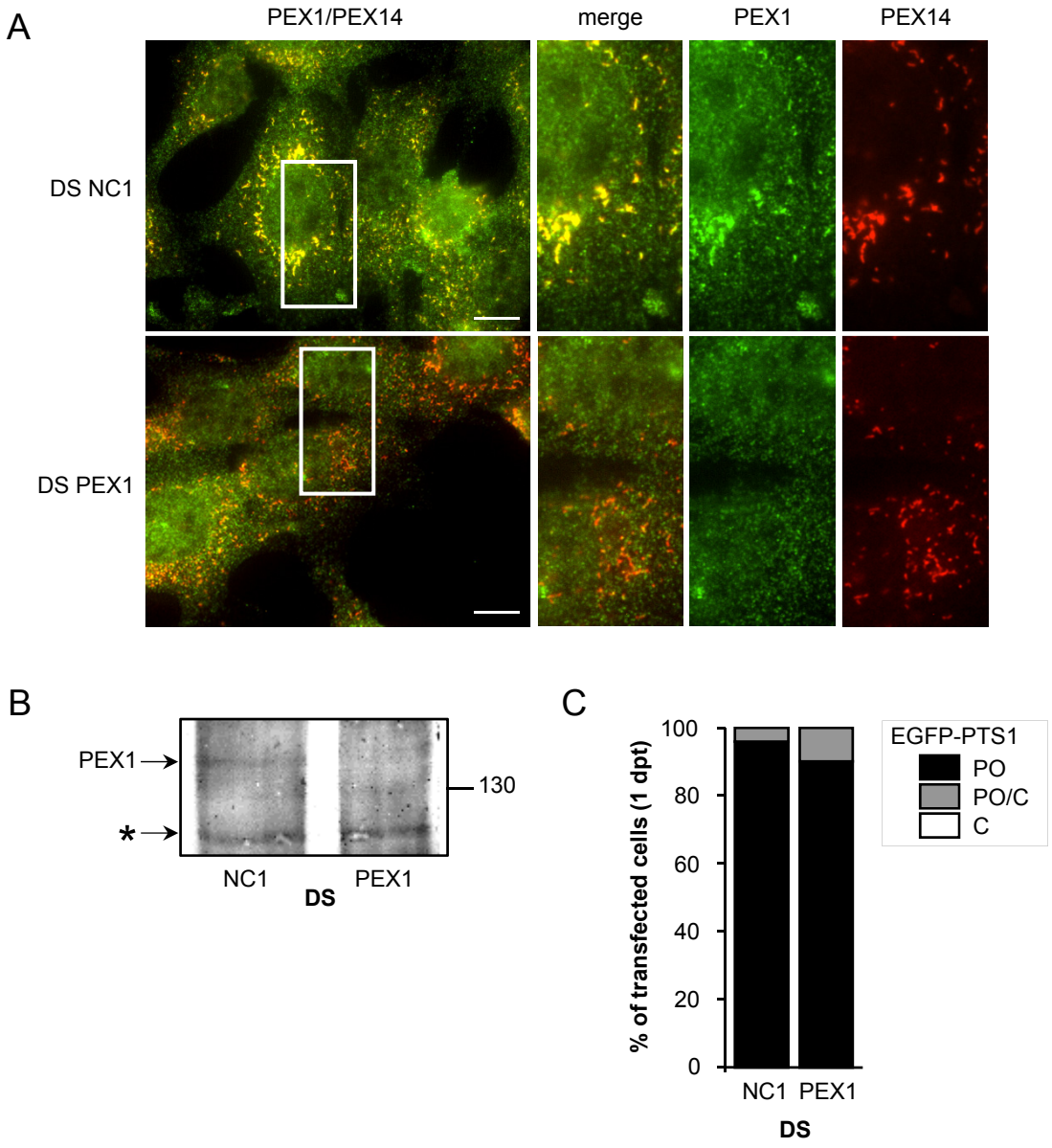
A
PEX1/PEX14
merge
PEX1
PEX14
DS NC1
DS PEX1
B
PEX1
*
130
NC1
PEX1
DS
C
% of transfected cells (1 dpt)
100
80
60
40
20
0
NC1
PEX1
DS
EGFP-PTS1
PO
PO/C
C

Figure S19

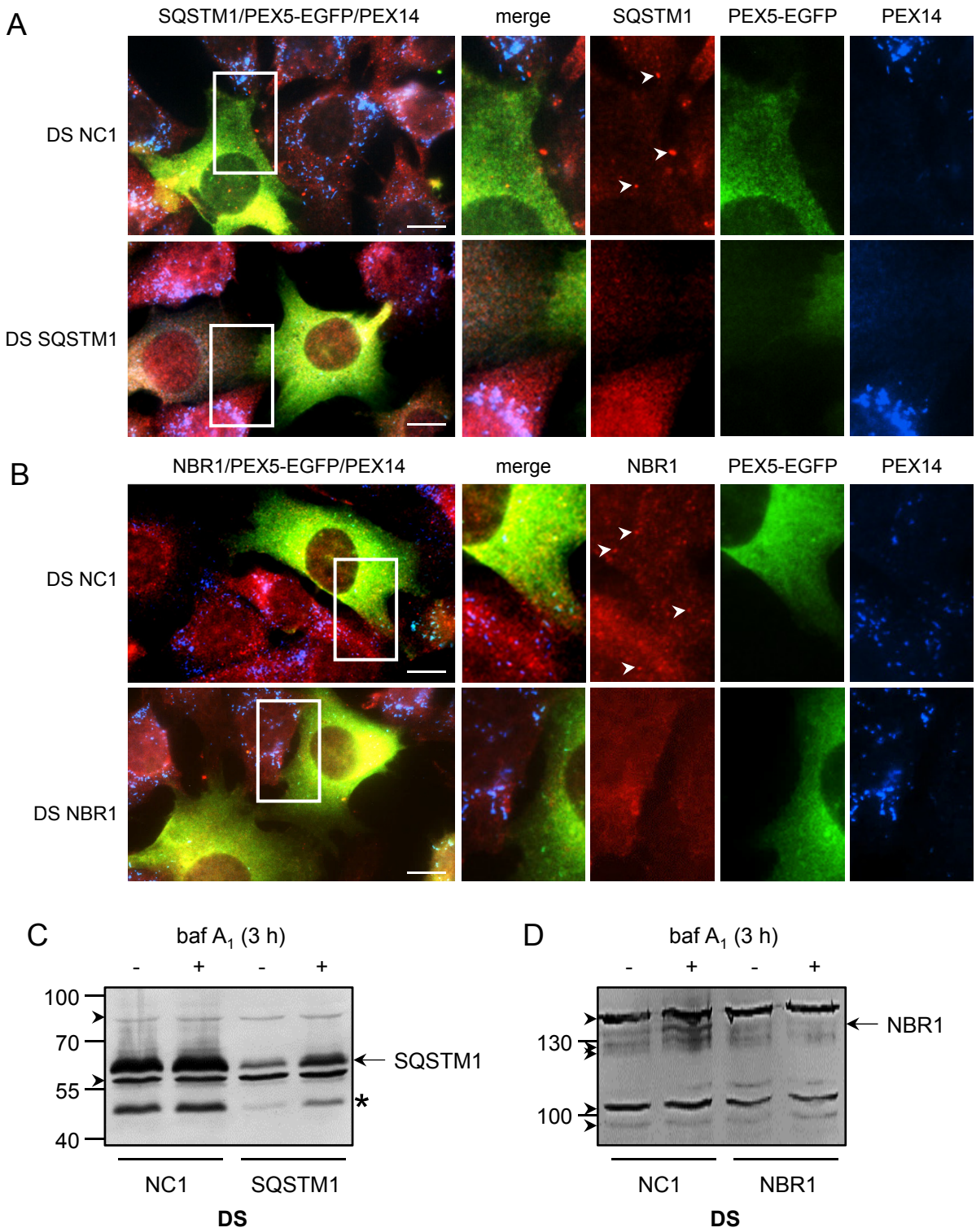
A
SQSTM1/PEX5-EGFP/PEX14
merge
SQSTM1
PEX5-EGFP
PEX14
DS NC1
DS SQSTM1
B
NBR1/PEX5-EGFP/PEX14
merge
NBR1
PEX5-EGFP
PEX14
DS NC1
DS NBR1
C
baf A1 (3 h)
- + - +
100
70
55
40
SQSTM1
*
NC1
SQSTM1
DS
D
baf A1 (3 h)
- + - +
130
100
NBR1
NC1
NBR1
DS

Figure S20

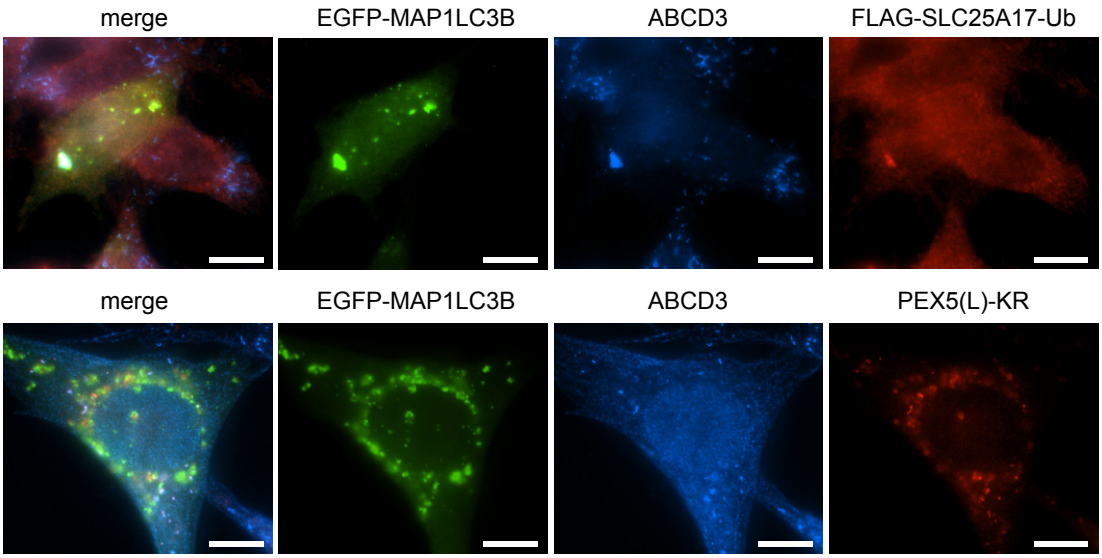
merge
EGFP-MAP1LC3B
ABCD3
FLAG-SLC25A17-Ub
merge
EGFP-MAP1LC3B
ABCD3
PEX5(L)-KR

Figure S21

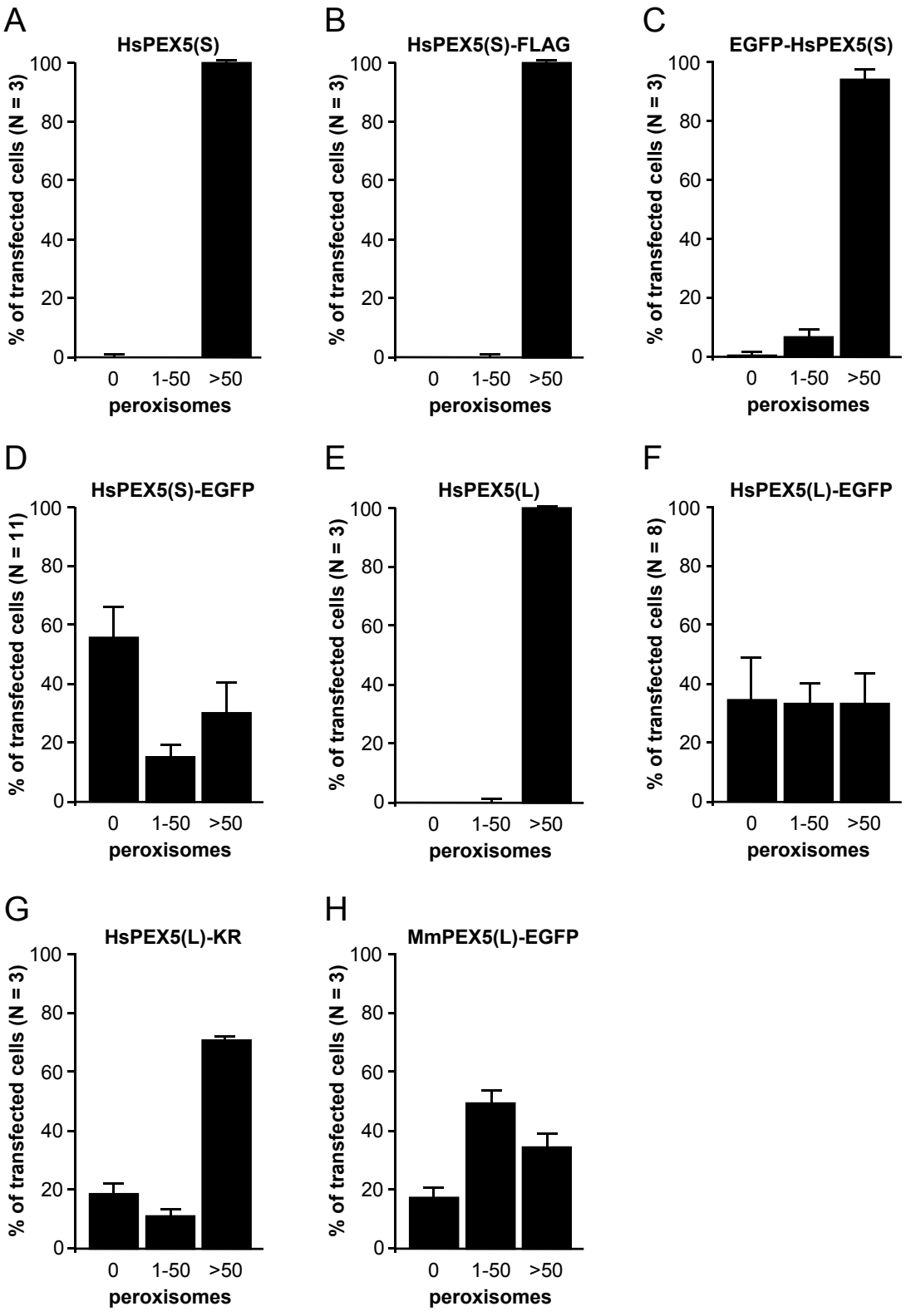
A
HsPEX5(S)
% of transfected cells (N = 3)
B
HsPEX5(S)-FLAG
% of transfected cells (N = 3)
C
EGFP-HsPEX5(S)
% of transfected cells (N = 3)
D
HsPEX5(S)-EGFP
% of transfected cells (N = 11)
E
HsPEX5(L)
% of transfected cells (N = 3)
F
HsPEX5(L)-EGFP
% of transfected cells (N = 8)
G
HsPEX5(L)-KR
% of transfected cells (N = 3)
H
MmPEX5(L)-EGFP
% of transfected cells (N = 3)
0
20
40
60
80
100
0
1-50
>50
peroxisomes

Figure S22

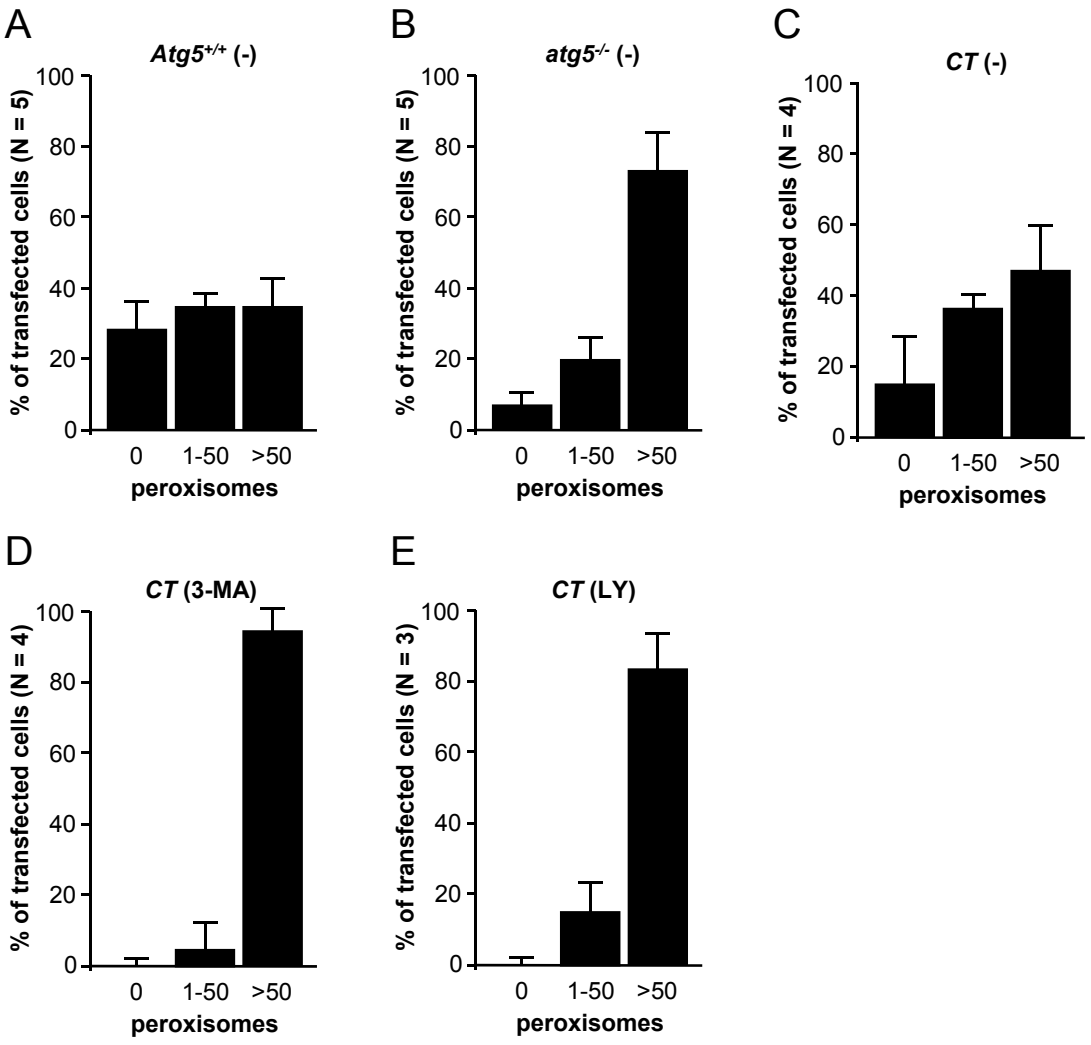
A
Atg5+/+ (-)
% of transfected cells (N = 5)
100
80
60
40
20
0
0
1-50
>50
peroxisomes
B
atg5-/- (-)
% of transfected cells (N = 5)
peroxisomes
C
CT (-)
% of transfected cells (N = 4)
peroxisomes
D
CT (3-MA)
% of transfected cells (N = 4)
peroxisomes
E
CT (LY)
% of transfected cells (N = 3)
peroxisomes

Figure S23

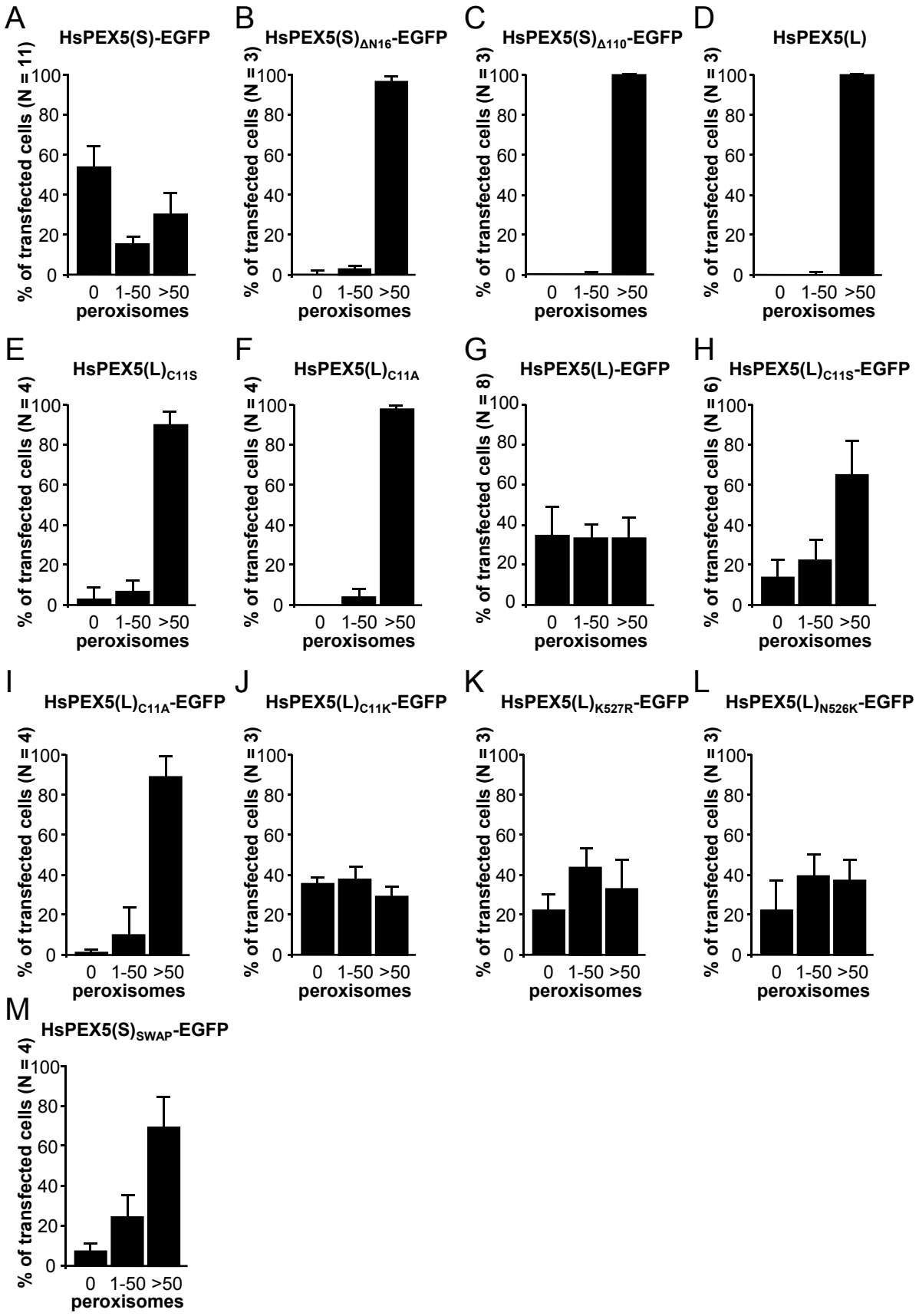
A
HsPEX5(S)-EGFP
% of transfected cells (N = 11)
B
HsPEX5(S)ΔN16-EGFP
% of transfected cells (N = 3)
C
HsPEX5(S)Δ110-EGFP
% of transfected cells (N = 3)
D
HsPEX5(L)
% of transfected cells (N = 3)
E
HsPEX5(L)C11S
% of transfected cells (N = 4)
F
HsPEX5(L)C11A
% of transfected cells (N = 4)
G
HsPEX5(L)-EGFP
% of transfected cells (N = 8)
H
HsPEX5(L)C11S-EGFP
% of transfected cells (N = 6)
I
HsPEX5(L)C11A-EGFP
% of transfected cells (N = 4)
J
HsPEX5(L)C11K-EGFP
% of transfected cells (N = 3)
K
HsPEX5(L)K527R-EGFP
% of transfected cells (N = 3)
L
HsPEX5(L)N526K-EGFP
% of transfected cells (N = 3)
M
HsPEX5(S)SWAP-EGFP
% of transfected cells (N = 4)
0 1-50 >50
peroxisomes

Figure S24

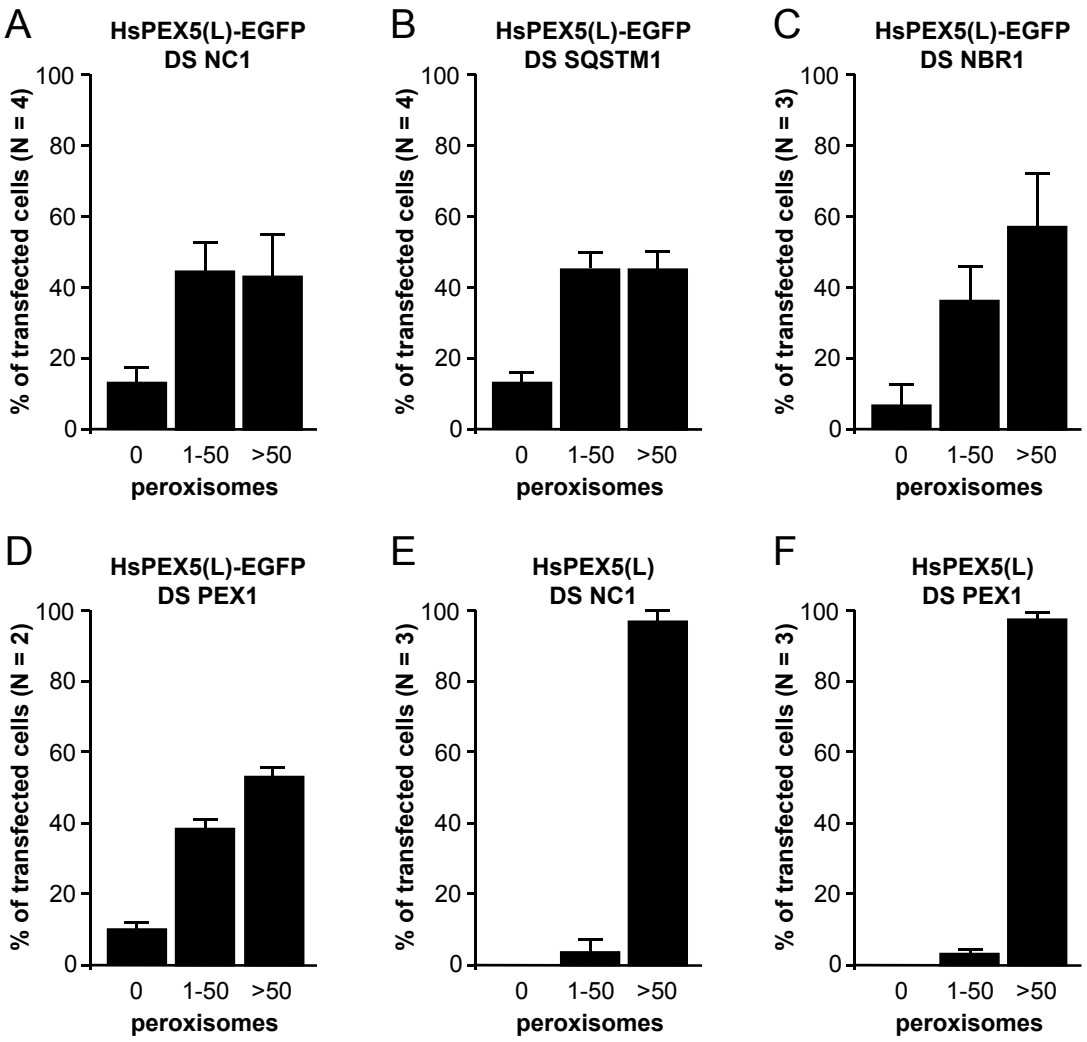
A
HsPEX5(L)-EGFP
DS NC1
% of transfected cells (N = 4)
B
HsPEX5(L)-EGFP
DS SQSTM1
% of transfected cells (N = 4)
C
HsPEX5(L)-EGFP
DS NBR1
% of transfected cells (N = 3)
D
HsPEX5(L)-EGFP
DS PEX1
% of transfected cells (N = 2)
E
HsPEX5(L)
DS NC1
% of transfected cells (N = 3)
F
HsPEX5(L)
DS PEX1
% of transfected cells (N = 3)
0
20
40
60
80
100
0
1-50
>50
peroxisomes

# Materials S1

## Description of the non-commercial plasmids used in this study

Unless indicated otherwise, all PEX5 constructs described below encode the human ortholog of this peroxin. The vectors encoding (cytosolic) KR (pMF1755), PEX5(L) (pMF961), PEX5(L)$_{C11K}$ (pMF1579), PEX5(L)$_{N526K}$ (pMF1698), PEX5(S) (pMF106), HsPMP34 (pBS-HsPMP34), or PEX5(S)$_{\Delta C299}$-PEX5L/PEX5R$_{\Delta N326}$-EGFP (pLA142) have been described elsewhere.[1-8] The plasmids encoding myc-tagged MmPEX5(L) (pLA141), GFP-LC3, LAMP1-EGFP, or LAMP2A-EGFP were acquired from Dr. M. Baes (KU Leuven, Belgium), Dr T. Yoshimori (National Institute of Genetics, Japan), Dr. T. Voets (KU Leuven, Belgium), and Dr. S. M. Di Pietro (Colorado State University, CO, USA), respectively. The plasmid encoding FLAG-PMP34-Ub (pMN19) was generated in 2 steps: first, *Eco*RI/*Sal*I-flanked Ub-encoding cDNA was isolated from human liver cDNA (TaKaRa, 637205) by PCR (primers: UbfwEcoRI and UbrvSalI) and cloned into an *Eco*RI/*Sal*I-restricted pCMV-Tag 2B vector to yield a plasmid encoding FLAG-Ub (pEA7); second, pMN19 was constructed by amplification of the *PMP34* cDNA by PCR (template: pBS-HsPMP34; primers: PMP34fwBamHI and PMP34rvEcoRI) and cloning the *Bam*HI/*Eco*RI-digested PCR product into the *Bam*HI/*Eco*RI-cut pEA7. The construct encoding human PEX5(L)-KR (pMF1758) was generated by cloning the *Sal*I/*Bgl*II-restricted PEX5(L)-coding PCR product (template pMF961; primers: PEX5fwSalI and PEX5rvBglII), and KR from the *Bam*HI/*Not*I-digested pKillerRed-dMito vector, into *Sal*I/*Not*I-restricted pEGFP-N1 via a 3-point ligation procedure. Also the plasmids encoding PEX5(L)-HaloTag (pMF1677) and HsHAO2 (hydroxyacid oxidase 2)-HaloTag (pMF1633; HaloTag-PTS1) were generated via a 3-point ligation procedure: pMF1677 was generated by cloning a *Sal*I/*Bgl*II-restricted PEX5-encoding PCR fragment (template: pMF961; primers: PEX5fwSalI and PEX5BglIIrv) and a *Bam*HI/*Not*I-restricted HaloTag-encoding PCR fragment (template: pHT2; primers: pHT2fw

and pHT2rvNot) into *Sal*I/*Not*I-restricted pEGFP-N1; and pMF1633 was generated by cloning a *Hin*dIII/*Bam*HI-restricted HaloTag-encoding PCR fragment (template: pHT2; primers: pHT2fwHindIII and pHT2rvBamHI) and a *Bam*HI/*Not*I-restricted HAO2-encoding PCR fragment (template: human liver cDNA; primers: HAO2fwBamHI and HAO2rvNotI) into *Hin*dIII/*Not*I-restricted pEGFP-N1. The bicistronic construct encoding peroxisomal roGFP2 and human PEX5(L)$_{C11S}$ (pDC3) was constructed by amplifying the corresponding PEX5(L)$_{C11S}$ cDNA fragment by PCR (template pMF1679[7]; primers: PEX5fwBglII3 and PEX5rvSalI2) and cloning the *Bgl*II/*Sal*I-digested PCR product into the *Bgl*II/*Sal*I-restricted pIRES2-roGFP2-PTS1 vector.[9] The plasmids coding for nontagged PEX5(S) (pMN56), PEX5(L) (pMN57), PEX5(L)$_{C11S}$ (pMN53), and PEX5(L)$_{C11A}$ (pMN64) were generated via amplification of the corresponding cDNAs via PCR (templates: pMF106 (pMN56), pMF961 (pMN57), pDC3 (pMN53), and pMN57 (pMN64); primers: PEX5fwBglII1 and PEX5rvNotI (pMN56, pMN57, pMN53), and PEX5$_{C11A}$fwBglII and PEX5rvNotI (pMN64)) and cloning the *Bgl*II/*Not*I-restricted PCR products into *Bgl*II/*Not*I-digested pEGFP-N1. The plasmids encoding EGFP fused to the C terminus of either PEX5(S) (pLA138), PEX5(L) (pMN65), PEX5(L)$_{C11S}$ (pMN54), PEX5(L)$_{C11A}$ (pMN63), PEX5(L)$_{C11K}$ (pMN75), PEX5(S)$_{\Delta N10}$ (pMF908), PEX5(S)$_{\Delta N110}$ (pMF916), and PEX5(L)$_{N526K}$ (pMN77) were constructed by amplifying the corresponding *PEX5* cDNAs via PCR (templates: pMN57 (pMN65), pMF1579 (pMN75), pDC3 (pMN54), pMN53 (pMN63), pMF106 (pLA138, pMF908, pMF916) and pMF1698 (pMN77); primers: PEX5fwBglII2 and PEX5rvSalI1 (pLA138), PEX5fwBglII1 and PEX5rvSalI3 (pMN65, pMN54, pMN75, pMN77) PEX5$_{C11A}$fwBglII and PEX5rvSalI3 (pMN63), PEX5$_{\Delta N10}$fwBglII and PEX5rvSalI3 (pMF908), PEX5$_{\Delta N110}$fwBglII and PEX5rvSalI3 (pMF916)) and cloning the *Bgl*II/*Sal*I-digested PCR products into the *Bgl*II/*Sal*I-restricted pEGFP-N1 vector. The plasmid encoding PEX5(L)-mCherry (pMN78) was generated by replacing the *Sal*I/*Not*I-restricted EGFP cassette by a *Sal*I/*Not*I-restricted

mCherry cassette (this cassette was amplified by PCR (template: pJ1:PG27188 (DNA2.0); primers: mCherrySalIfw and mCherryNotIrv)). The plasmid encoding PEX5(S)$_{N489K}$-EGFP (pMN80) was generated by cloning the *Hin*dIII/*Not*I-restricted insert of pMN77 into the *Hin*dIII/*Not*I-restricted backbone of pMN56. To generate the plasmid coding for the fusion protein PEX5(S)$_{\Delta C299}$-PEX5L/PEX5R$_{\Delta N326}$-EGFP (pMN70), the *Bgl*II/*Sal*I-restricted PCR product (template: pLA142; primers: PEX5fwBglII1 and PEX5RrvSalI) was cloned into the *Bgl*II/*Sal*I-digested pEGFP-N1 vector. The plasmid encoding human PEX5(L)$_{K527R}$-EGFP (pMN71) was generated by amplifying the cDNA encoding PEX5(L)$_{K527R}$ via fusion PCR and cloning the corresponding *Bgl*II/*Sal*I-digested PCR product into the backbone fragment of *Bgl*II/*Sal*I-restricted pEGFP-N1. The fusion PCR product was generated as follows: in a first PCR reaction, 2 PCR fragments (template: pMN57; primers PEX5fwBglII1 and PEX5$_{K527R}$rv (fragment 1), PEX5$_{K527R}$fw and PEX5rvSalI3 (fragment 2)) were generated; these fragments were fused and used as template in a second PCR reaction generating the final cDNA (primers: PEX5fwBglII1 and PEX5rvSalI3). The plasmid encoding MmPEX5(L)-EGFP (pMN62) was generated by cloning the *Nhe*I/*Sal*I digested MmPEX5(L) PCR product (template: pLA141; primers: PEX5fwNheI and PEX5rvSalI4) into the *Nhe*I/*Sal*I-restricted backbone fragment of pEGFP-N1. The pGEM-based vectors encoding EGFP-tagged PEX5(L) (pMN66), PEX5(L)$_{C11K}$ (pMN76), PEX5(L)$_{C11S}$ (pMN67) and PEX5(L)$_{C11A}$ (pMN68) were generated by amplifying the corresponding cDNAs via fusion PCR and cloning the *Sal*I/*Bgl*II-restricted PCR products into the backbone fragment of a *Sal*I/*Bam*HI-digested pGEM-4 vector. The fusion PCR products were generated as follows: in a first PCR reaction, 2 PCR fragments (template: pMN65 (pMN66), pMN54 (pMN67), pMN63 (pMN68), pMF1579, and pMN65 (pMN76); primers: PEX5fwSalI and PEX5fusionrv (fragment 1), PEX5fusionfw and EGFPrvBglII (fragment 2)) were generated; these fragments

were fused and used as template in a second PCR reaction generating the final cDNAs (primers: PEX5fwSalI and EGFPrvBglII).

***References cited in the upper paragraph***


1. Wylin T, Baes M, Brees C, Mannaerts GP, Fransen M, Van Veldhoven PP. Identification and characterization of human PMP34, a protein closely related to the peroxisomal integral membrane protein PMP47 of *Candida boidinii*. Eur J Biochem 1998; 258: 332-338.
2. Kabeya Y, Mizushima N, Ueno T, Yamamoto A, Kirisako T, Noda T, Kominami E, Ohsumi Y, Yoshimori T. LC3, a mammalian homologue of yeast Apg8p, is localized in autophagosome membranes after processing. EMBO J 2000; 19: 5720-5728.
3. Amery L, Sano H, Mannaerts GP, Snider J, Van Looy J, Fransen M, Van Veldhoven PP. Identification of PEX5-related novel peroxisome-targeting signal 1 (PTS1)-binding proteins in mammals. Biochem J 2001; 357: 635-646.
4. Fransen M, Brees C, Ghys K, Amery L, Mannaerts GP, Ladant D, Van Veldhoven PP. Analysis of mammalian peroxin interactions using a non-transcription-based bacterial two-hybrid assay. Mol Cell Proteomics 2002; 1: 243-252.
5. Gouveia AM, Guimarães CP, Oliveira ME, Reguenga C, Sá-Miranda C, Azevedo JE. Characterization of the peroxisomal cycling receptor Pex5p import pathway. Adv Exp Med Biol 2003; 544: 219-220.
6. Carvalho AF, Grou CP, Pinto MP, Alencastre IS, Costa-Rodrigues J, Fransen M, Sá-Miranda C, Azevedo JE. Functional characterization of two missense mutations in Pex5p - C11S and N526K. Biochim Biophys Acta 2007; 1773: 1141-1148.
7. Grou CP, Carvalho AF, Pinto MP, Huybrechts SJ, Sá-Miranda C, Fransen M, Azevedo JE. Properties of the ubiquitin-Pex5p thiol ester conjugate. J Biol Chem 2009; 284: 10504-10513.

8. Ivashchenko O, Van Veldhoven PP, Brees C, Ho YS, Terlecky SR, Fransen M. Intraperoxisomal redox balance in mammalian cells: oxidative stress and interorganellar crosstalk. Mol Biol Cell 2011; 22: 1440-1451.

9. Apanasets O, Grou CP, Van Veldhoven PP, Brees C, Wang B, Nordgren M, Dodt G, Azevedo JE, Fransen M. PEX5, the shuttling import receptor for peroxisomal matrix proteins, is a redox-sensitive protein. Traffic 2014; 15: 94-103.

**Table S1.** List of oligonucleotides used in this study.

| Name | Nucleotide sequence |
|---|---|
| EGFPrvBglII | 5’-gagaagatctttacttgtacagctcgtcc-3’ |
| HAO2fwBamHI | 5’-gggggatccatgtccttggtgtgtctg-3’ |
| HAO2rvNotI | 5’-ggggcggccgcttacagcctggaaaactggac-3’ |
| mCherryNotIrv | 5’-ggcggggcggccgcttacttgtacagctcgtcc-3’ |
| mCherrySalIfw | 5’-gccggtcgaccaccggtcgccaccatggtgagcaagggcgag-3’ |
| PEX5BglIIrv | 5’-gggagatctccctggggcaggccaaacatag-3’ |
| PEX5C11AfwBglII | 5’-ggggagatctaccatggcaatgcgggagctggtggaggccgaa**GC**cgggggtgccaacc-3’ |
| PEX5fusionfw | 5’-ccagctctcgacggtaccgcggg-3’ |
| PEX5fusionrv | 5’-gtaccgtcgagagctggggcaggccaaac-3’ |
| PEX5fwBglII1 | 5’-gggagatctaccatggcaatgcgggagctg-3’ |
| PEX5fwBglII2 | 5’-gggagatctatggcaatgcgggagctggtg-3’ |
| PEX5fwBglII3 | 5’-cgagatctgtatggcaatgcgggagctgg-3’ |
| PEX5fwNheI | 5’-cggcgggctagcaccatggcaatgcgggagctg-3’ |
| PEX5fwSalI | 5’-ggcgggtcgacgtcaccatggcaatgcgggag-3’ |
| PEX5ΔN10fwBglII | 5’-gggagatctaccatggcaatgaagctcgccgggcac-3’ |
| PEX5ΔN110fwBglII | 5’-gggagatctaccatggcagacttggccttgtct-3’ |
| PEX5K527Rfw | 5’-gctgtggaata**G**gctaggcgccaccctg-3’ |
| PEX5K527Rrv | 5’-cctagc**C**tattccacagcaaatagtcattg-3’ |
| PEX5rvBglII | 5’-gggagatctccctggggcaggccaaacatag-3’ |
| PEX5rvNotI | 5’-gggggcggccgctcactggggcaggccaaac-3’ |
| PEX5rvSalI1 | 5’-ccttcgtcgactggggcaggccaaacatag-3’ |
| PEX5rvSalI2 | 5’-gcccgtcgacctgtcactggggcaggccaaac-3’ |
| PEX5rvSalI3 | 5’-gagaggtcgacagctggggcaggccaaacatagt-3’ |
| PEX5rvSalI4 | 5’-gagaggtcgacagctggggcaggccaaacatag-3’ |

| | |
|---|---|
| PEX5RrvSalI | 5’-gggggtcgactgaggatccaagttgaaagctc-3’ |
| pHT2fw | 5’-gggggtaccggatccgatggggtccgaaatcggtacaggc-3 |
| pHT2fwHindIII | 5’-gggaagcttaccatggggtccgaaatcggtac-3’ |
| pHT2rvBamHI | 5’-gggggatccgccgccggccagcccggggag-3’ |
| pHT2rvNotI | 5’-agggaagcggccgcctactt-3’ |
| PMP34fwBamHI | 5’-gagcggatccatggcttccgtgctgtcc-3’ |
| PMP34rvEcoRI | 5’-gcggaattcgcctccgtgttggtgtgcacgctt-3’ |
| UbfwEcoRI | 5’-ggcgcgaattcatgcagatcttcgtgaagactc-3’ |
| UbrvSalI | 5’-gttttgtcgacctacccacctctgagacggagcac-3’ |

2 Restriction sites are underlined. Nucleotides in bold capital letters represent the $C_{11}A$ and $K_{527}R$ mutations.